Identification of dual Sigma1 receptor modulators/Acetylcholinesterase inhibitors with antioxidant and neurotrophic properties, as neuroprotective agents.

Marta Rui[1], Giacomo Rossino[1], Stefania Coniglio[1], Stefania Monteleone[2,3], Arianna Scuteri[4], Alessio Malacrida[4], Daniela Rossi[1], Laura Catenacci[1], Milena Sorrenti[1], Mayra Paolillo[1], Daniela Curti[5], Letizia Venturini[6], Dirk Shepmann[7], Bernhard Wünsch[7], Klaus R. Liedl[2], Guido Cavaletti[4], Vittorio Pace[8], Ernest Urban[8], Simona Collina[1]*

[1] *Department of Drug Sciences, Medicinal Chemistry, Pharmaceutical Technology and Pharmacological sections, University of Pavia, Viale Taramelli 6 and 12, 27100 Pavia (Italy).*

[2] *Institute of General, Inorganic and Theoretical Chemistry, University of Innsbruck, Innrain 80-82, 6020 Innsbruck (Austria).*

[3] *Department of Pharmaceutical Chemistry, Philipps-University Marburg, Marbacher Weg 6, 35032 Marburg (Germany).*

[4] *School of Medicine and Surgery, University Milano-Bicocca, via Cadore 48, 20900 Monza (Italy).*

[5] *Department of Biology and Biotechnology "L. Spallanzani", Lab. of Cellular and Molecular Neuropharmacology, University of Pavia, Via Ferrata 9, 27100 Pavia (Italy).*

[6] *Department of Internal Medicine and Therapeutics, University of Pavia, Via Taramelli 24, 27100 Pavia (Italy).*

[7] *Institute of Pharmaceutical and Medicinal Chemistry, University of Muenster, Correnstrasse 48, 48149 Muenster (Germany).*

[8] *Department of Pharmaceutical Chemistry, University of Vienna, Althanstrasse 14, 1090 Vienna (Austria).*

Abstract

This manuscript deals with the design, synthesis and evaluation of dual Sigma 1 Receptor (S1R) modulators/Acetylcholinesterase (AChE) inhibitors endowed with antioxidant and neurotrophic properties, potentially able to counteract neurodegeneration, namely the progressive loss of structure and/or function of neurons. The compounds based on arylalkylaminoketone scaffold integrate the pharmacophoric elements of (R)-RC-33, a S1R modulator developed by us, donepezil, a well-known AChE inhibitor, and curcumin, a natural antioxidant compound with neuroprotective properties. A small library of compounds was synthesized and preliminary *in vitro* screening performed. Some compounds showed good S1R binding affinity, selectivity towards S2R and *N*-Methyl-D-Aspartate (NMDA) receptor, AChE relevant inhibiting activity and are potentially able to bypass the BBB, as predicted by the *in silico* study. For the hits **10** and **20**, the antioxidant profile was assessed in SH-SY5Y human neuroblastoma cell lines by evaluating their protective effect against H_2O_2 cytotoxicity and reactive oxygen species (ROS) production. Tested compounds resulted effective in decreasing ROS production, thus ameliorating the cellular survival. Moreover, compounds **10** and **20** showed to be effective in promoting the neurite elongation of Dorsal Root Ganglia (DRG), thus demonstrating a promising neurotrophic activity. Of note, the tested compounds did not show any cytotoxic effect at the concentration assayed. Relying on these encouraging results, both compounds will undergo a structure optimization program for the development of therapeutic candidates for neurodegenerative diseases treatment.

Keywords: Neuroprotective agents, Sigma1 Receptor, acetylcholinesterase inhibitors, antioxidant properties, neurotrophic properties

1. Introduction

The progressive loss of structure and/or function of neurons, within the Central Nervous System (CNS), is the prototypical event leading to neurodegeneration, which is an aspect underpinning a heterogeneous group of disorders [1-2]. The World Health Organization (WHO) recently reported that neurodegenerative diseases, *i.e.* Alzheimer's (AD), Parkinson's (PD), Amyotrophic Lateral Sclerosis (ALS) and Multiple Sclerosis (MS), are one of the main causes of death worldwide, causing the death of 6.8 million people annually (Figure 1) [3-5]. Moreover, the treatment options of neurodegenerative diseases are meagre, since only few molecules able to attenuate the devastating outcome and/or to limit the progression of the diseases are available and thus, there is an urgent need of effective therapies [6]. Neurodegenerative disorders have a multifactorial origin, being associated with both environmental factors, such as smoking, stress and the use of pesticides, and specific genetic variations, leading to alteration of several molecular cascades (Figure 1) [7-8]. Dysfunction of neurotransmitter pathways (*i.e.* acetylcholine or dopamine systems) can sometimes occur together with abnormal structure and/or accumulation of proteins – *i.e.* tau protein hyperphosphorylation, β-amyloid accumulation, further aggravating the pathological condition [9-12]. An important hallmark of neurodegeneration conditions is an over-production of Reactive Oxygen Species (ROS) due to alterations of mitochondrial respiratory chain activity [13-14].

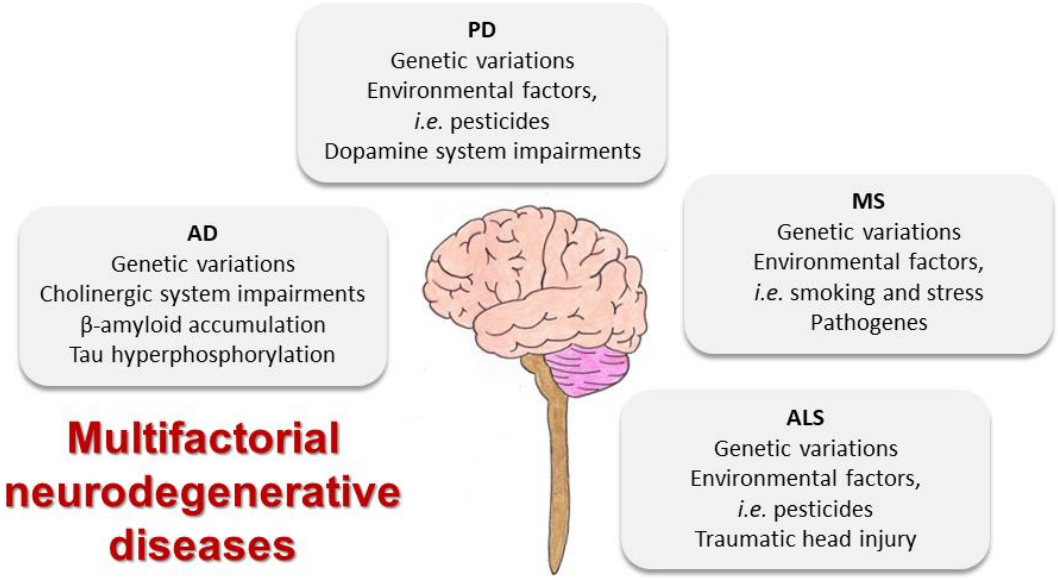

Figure 1. Some aetiological factors that promote multifactorial neurodegenerative diseases.

In our continuing efforts towards the design and development of new molecular entities able to counteract neurodegeneration, we prepared a compound library targeting Sigma 1 Receptor (S1R). Among our molecules, (R)-RC-33 has been identified as the most most promising one, being characterized by an excellent affinity and selectivity towards S1R over S2R (Ki S1 = 1.8 ± 0.1 nM; Ki S2 = 45 ± 16 nM) and a high metabolic stability in several biological matrices [15]. Furthermore, we reported its ability in promoting the differentiation and the neurite elongation in rat Dorsal Root Ganglia (DRG) experimental model, which is a well-accepted simple method to screen neurotoxic or neuroprotective effect of a drug [16].

Aiming at further exploring the structural insights of our in-house library and keeping in mind that neurodegeneration is characterized by multifactorial aspects, multi-target drugs (MTDs) may be a good therapeutic opportunity [17]. Accordingly, herein we report the design, synthesis, and biological evaluation of a series of dual ligands, able to modulate S1R, acting as acetylcholinesterase (AChE) inhibitors and endowed with antioxidant properties.

The rationale for such a combination is that S1R modulators may be effective neuroprotective agents, since under pathological conditions S1R operates as chaperone modulating different proteins, restoring the calcium homeostasis and controlling the generation of ROS, thus preventing cellular damage [18-24], while AChE inhibitors and antioxidant compounds could restore memory and cognition by stimulating alive neurons. Our inspiring molecules were RRC-33, donepezil and curcumin (Cur). Donepezil (Figure 2) is an AChE inhibitor, effective against cognitive impairment, a common feature of neurodegenerative diseases, by restoring the physiological amount of acetylcholine [25-26]. Cur (Figure 2) is an effective ROS scavenging compound [27]. It is the main yellow-colored pigment of *Curcuma longa*, historically employed in Ayurvedic medicine [28]. Although its numerous drawbacks linked to its solubility, instability in physiological fluids, and low bioavailability [29], Cur possesses a wide spectrum of action including antioxidant activities, which may be useful to counteract neurodegenerative diseases [30-32]. We speculated that the a fragment-based approach, which combines the structural features of (R)-RC-33, donepezil and Cur, could lead to the identification of a S1R modulator endowed with AchE inhibitor effect and antioxidant properties (Figure 2).

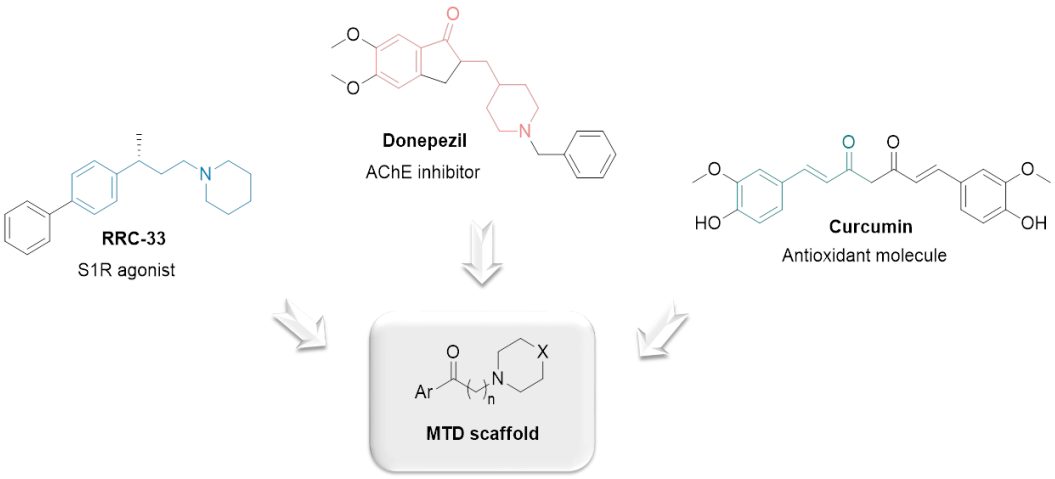

Figure 2. MTD scaffold merges the key functional groups of S1R agonists, AChE inhibitors and curcumin.

Relying on the above considerations and on our experience on S1R modulators, herein we present our efforts in the design, synthesis and biological evaluation of a new series of dual compounds combining S1R modulation with AChE inhibition. The in vitro and in silico studies revealed the most promising molecules, which were further investigated by analysing their antioxidant and neurotrophic properties.

2. Results and discussion

2.1. Chemistry

We prepared a new compound series, characterized by an arylalkylamineketone scaffold with three elements of structural diversity, *i.e.* the aromatic ring, the aminic moiety and the length of the linker between the aromatic and the aminic portions (Figure 2). The conceived arylalkylamineketone scaffold allowed improving synthetic feasibility and chemical tractability by removal of chiral center present in the inspiring S1R modulator (R)-RC-33.

Compounds were synthesized by following the general synthetic route outlined in Scheme 1 and Scheme 2.

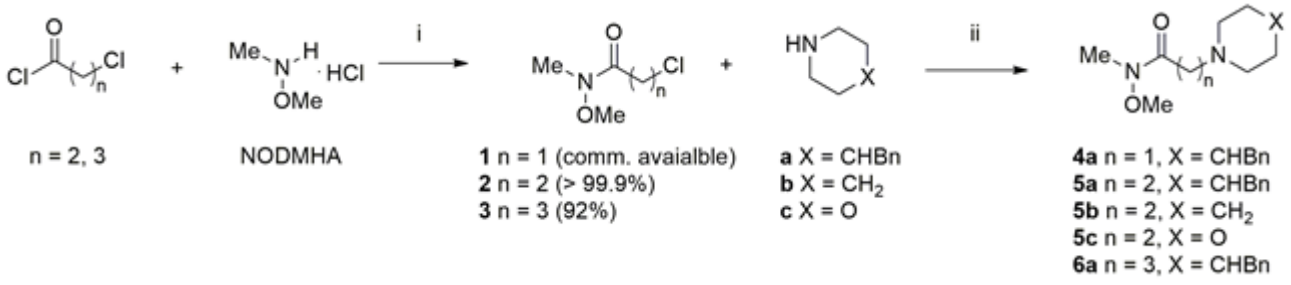

Scheme 1: Weinreb amide formation and nucleophilic substitution. Reagents and reaction conditions: i) K_2CO_3, Et_2O/H_2O, r.t.; ii) K_2CO_3, ACN, r.t.

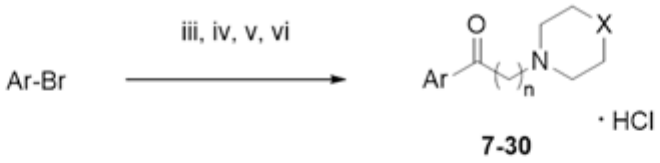

7-30

Cmpd	Ar	n	X	Yield (%)
7	phenyl	1	CHBn	40
8	4-methoxyphenyl			37
9	3-methoxyphenyl			48
10	naphth-2-yl			54
11	6-methoxynaphth-2-yl			49
12	4-biphenyl			33
13	Phenyl	2	CHBn	28
14	4-methoxyphenyl			25
15	naphth-2-yl			22
16	4-biphenyl			22
17	phenyl	2	CH_2	29
18	4-methoxyphenyl			27
19	naphth-2-yl	2	CH_2	23
20	4-biphenyl			35
21	Phenyl	2	O	30
22	4-methoxyphenyl			38
23	naphth-2-yl			41
24	4-biphenyl			37
25	phenyl	3	CHBn	31
26	4-methoxyphenyl			30
27	3-methoxyphenyl			33
28	naphth-2-yl			41
29	6-methoxynaphth-2-yl			25
30	4-biphenyl			26

Scheme 2: Lithiated arene formation and quenching with the corresponding Weinreb amide. Reagents and reaction conditions: iii) *t*-BuLi, THF, -78 °C iv) Weinreb amide (**4a**, **5a-c** or **6a**), -78 °C; v) H_2O; vi) HCl (1M in Et_2O), Et_2O.

A divergent synthesis has been adopted to access the desired products in good yields and in few steps. Target compounds **7**-**30** were obtained via Weinreb ketone synthesis from key intermediates **4a**, **5a-c** and **6a**, which in turn were prepared through: i) the Weinreb amide formation and ii) a nucleophilic substitution (Scheme 1). Specifically, the starting acyl chlorides were easily converted into the desired β and γ chloro Weinreb amides, using the amine *N*,*O*-dimethylhydroxyamine hydrochloride (NODMHA), in the presence of a basic reagent, K_2CO_3. The reactions performed in a mixture of ether and water (in equal amount) were stirred for 24 h. A simple extraction provided compounds **2-3** in excellent yields. This reaction was not applied for achieving intermediate **1**, since it is commercial available. Accordingly, the Weinreb amides were subjected to a nucleophilic substitution, exploiting the chlorine as good leaving group. The reaction performed with the corresponding secondary amine (**a-c**), needed 24 h and the presence of K_2CO_3 as base to yield the crude α, β and γ amino Weinreb amides **4a**, **5a-c** and **6a**. An acid/base extraction was essential to obtain the key intermediates,

presenting 1 or 2 carbonaceous units, in modest/good yields. Conversely, **6a** required a purification through flash chromatography, since the starting material conversion into the desired products furnished some side products. Lastly, the smooth bromo-lithium exchange on the aryl bromide afforded the lithiated arene that, upon quenching with **4a**, **5a-c** and **6a**, gave the desired ketones **7-30** in good yields, after an adequate purification (Scheme 2). Specifically, the corresponding aryl bromide were lithiated, in anhydrous THF at -78 °C with *t*-butyl lithium. The subsequent addition of compounds **4a**, **5a-c** and **6a** and quenching with H_2O led to isolate crude compounds, which were purified through flash chromatography. All the potential MTD molecules **7-30** were obtained in a sufficient amount and with the appropriate degree of purity, as confirmed by IR, ^{1}H-NMR, ^{13}C-NMR and UPLC-MS analysis, as well as thermal analysis, for the following biological investigations. Preliminary solid-state characterization by DSC analysis revealed that all the compounds are crystalline anhydrous phases, with a well-defined melting point followed by sample decomposition, with the only exception of **28** which crystallized as solvatomorph.

2.2. Physicochemical and pharmacokinetic predictions

Molecular descriptors were computed to predict six physicochemical properties of each compound: (a) partition coefficient (ClogP); (b) distribution coefficient at pH 7.4 (ClogD); (c) molecular weight (MW); (d) topological polar surface area (TPSA); (e) number of hydrogen-bond donors (HBDs); and (f) acid dissociation constant (pKa). These parameters are the most representative features to determine the ADME profile, as well as the ability of a compound in reaching the CNS [33]. According to Wager *et al.* model, which is a well-established procedure broadly employed in academic and in industrial settings [34], a score – ranging from 0 to 1 - is attributed to each property, applying a monotonic decreasing function for ClogP, ClogD, MW, pKa, and HBD, whereas a hump function for TPSA (Table SI1). The summation of all these values gives access to a final score (0-6),

which can be defined as follows: i) 0-2, compound is unable to cross the BBB; ii) 2-5, compound may reach the CNS; iii) 5-6, compound effectively crosses the BBB [34]. Accordingly, we exploited this model to calculate the potential ability of compounds **7-30** in reaching the CNS (Table 1). For comparative purposes, we compared the obtained results with those of RRC-33 and Donepezil (Table 1, Table SI1), for which is known their good CNS distribution.

The tabulated results show that only four compounds (**18** and **21**-**23**) possess a score higher than 5, whereas the other ones possess values ranging from 2 to 5. Noteworthy, compounds **9**, **14**, **17**, **19**, **20** and **24** display a good score (> 4). Altogether these values reveal that all molecules **7**-**30** are able to reach the CNS. Moreover, reference compounds (R)-RC-33 and Donepezil show good scores (2.57 and 4.41, respectively) and this behaviour is in line with their *in vivo* CNS distribution, which was extensively confirmed by experimental data and clinical use.

2.3. Binding affinity, enzymatic studies, and structure-activity relationship (SAR) exploration

S1R and S2R binding site affinities of compounds **7-30** were measured through competition experiments, using radioligands. The assay for S1R was performed using homogenized guinea pig cerebral cortex membranes, in the presence of [^{3}H]-(+)-pentazocine, as a potent and selective S1R radioligand. Nonspecific binding values were determined using non-radiolabeled (+)-pentazocine and haloperidol in large excess. Conversely, homogenized rat liver membranes were adopted to evaluate the S2R binding values, employing [^{3}H]-DTG - a nonselective S2R radioligand - and, non-tritiated (+)-pentazocine to mask the S1R. Moreover, a high concentration of non-tritiated DTG was used to determine nonspecific binding values. Compounds with high affinity were tested three times. For compounds with low SR affinity, only one measure was performed. The SR affinities of compounds **7-30** towards both S1R and S2R are presented in Table 1.

Similar to reference compound RRC-33, almost all compounds possess a weak affinity for S2R, but only 12 compounds (**8**, **10**, **13-14**, **18**, **20**, **23-28**) over 24 present a Ki S1R lower than 50 nM. Altogether these results allow to draw some SAR considerations: i) the 4-methoxyphenyl ring seems to play a key role in the interaction with S1R, in fact molecules **8**, **14**, **18** and **26** belonging to the three different n series present a good Ki values (27, 11, 8 and 2.9 nM, respectively); ii) a longer linker guarantees the S1R binding, as it is evident in the 4-benzylpiperidine derivatives (**7-16** and **25-30**), which follow 1 = 2 < 3 n-scale in the interaction with S1R; iii). the length of the linker can limit the selectivity, indeed compounds belonging to the n = 3 series present a S2R/S1R ranging from 1.6 to 6.8 and thus, they may be considered as pan-SR modulators. Lastly, arylalkylamineketones possess a lower S1R affinity than (R)-RC-33 (Ki S1R = 1.8 nM), this difference may be associated to the presence of a novel pharmacophoric element, which can limit the interaction with the molecular target.

At the same time, we extended our study on the *N*-Methyl-D-Aspartate (NMDA) receptor, an ionotropic glutamate receptor, constituted by two subunits GluN1 and GluN2. NMDA receptor plays a relevant role in synaptic plasticity and synapse formation underlying memory and learning. An alteration of this neurotransmitter pathway causes an accumulation of glutamate in the synaptic terminations that promotes the GluN2 activation and thus, the long-term signal enhancement between two neurons. Moreover, the pathological triad, that involves mitochondrial dysfunction, loss of neuronal structures integrity, and disruption of excitation–transcription coupling, may be triggered. Accumulating evidence suggests that a negative modulation of this molecular target may contribute in slowing the progression of neuropathies [35]. Relying on these considerations, we evaluated the affinity of **7-30** towards GluN2 subunit of NMDA. Competitive binding assays on membrane extracts of L cells (tk-), stably transfected with a vector containing the genetic information of GluN1a and GluN2B subunits, were performed, using [^{3}H]-ifenprodil, a selective and potent GluN2 inhibitor

radioligand. Compounds with high affinity were tested three times. For compounds with low NMDA affinity, only one measure was performed. The results are reported in Table 1 and they show that **7-30** possess a weak affinity towards NMDA receptor, with the exception of compounds **8-10**, **13**, **25-29**, which show a Ki < 150 nM. These results highlight that the affinity towards NMDA receptor depends on the length of the spacer, in fact compounds belonging to the n = 3 series present good affinity towards GluN2 (20-117 nM). Conversely, molecules with 3 carbonaceous units between the aromatic portion and the aminic moiety are endowed with a negligible affinity for the ionotropic glutamate receptor, with the exception of compound **13** (Ki = 39 ± 2.1 nM). Lastly, molecules **7-12** show an intermediate behaviour, presenting a moderate binding affinity. These results did not discourage us, since the affinity towards NMDA receptor is not a necessary condition to define our compounds as MTDs. In fact, as aforementioned S1R can modulate the activity of several client proteins and NMDA receptor is a molecular target of S1R.

Compounds **7-30** were then tested for defining their potential to inhibit AChE. A spectrophotometric procedure was adopted, applying suitable modifications to the original Ellman's method [36-37]. An initial screening was performed, employing the target compounds at a concentration of 50 μM. The results of this assay are summarized in Table 1. Noteworthy, 10 compounds (**9-10**, **14-15**, **20**, **25-27**, **29-30**) over 24 possess a percentage of inhabitation ≥ 60%, whereas only five (**7-8**, **12**, **21** and **24**) can be considered inactive since they present a percentage of inhibition < 20%.

In the light of these data, for the most promising compounds, showing at a concentration of 50 μM an inhibition percentage more than 60%, the IC_{50} values were determined. Interestingly, all the tested compounds possess an IC_{50} lower than 25 μM, with the only exception of **9** (IC_{50} = 32.88 ± 1.77 μM) (Table 1). In particular, **27** and **29** result the most promising AChE inhibitors, with an IC_{50} of 7.64 ± 2.07 and 4.28 ± 0.23 μM, respectively.

From a structural point of view, the most interesting compounds are characterized by the presence of 4-benzylpiperidine, as aminic portion, with the exception of compound **20** that is characterized by a piperidine moiety. Moreover, molecules belonging to the n = 3 series (**25**-**27**, **29**-**30**) show greater anti-AChE effect; this inhibitory activity progressively decreases for β- and α-amino ketones, respectively (**9**-**10**, **14**-**15** and **20**). Basing on the obtained results we can conclude that both the 4-benzylpiperidine portion and the linker length have a crucial role for the anti-AChE activity, whereas no relation between the aromatic portion and the anti-AChE activity has been evidenced. Interestingly, RRC-33, the S1R reference compound, demonstrates no inhibition property against AChE (percentage of inhibition < 5%).

Table 1. Scores related to the potential ability of compounds 7-30 in crossing the BBB. Binding affinities towards NMDA, S1R and S2R and S1R selectivity (Ki S2R/Ki S1R). AchE inhibition activity and IC_{50} of the most promising compounds.

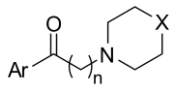

Cmpd	Score	Ki S1R (nM)	Ki S2R (nM)	S2R/S1R	Ki NMDA (nM)	% of inhibition (50 μM)	IC_{50} (nM)
7	3.47	75 ± 3.6	2.3 μM	30.7	215	5.65 ± 0.10	[b]
8	3.57	27 ± 1.2	2 μM	74	16 ± 1.2	8.21 ± 0.06	[b]
9	4.04	131 ± 15	1.5 μM	11.5	11 ± 0.4	75.50 ± 0.02	32.82 ± 1.77
10	3.02	27 ± 1.8	802	30	139 ± 11	87.40 ± 6.39	9.13 ± 2.24
11	3.42	286	1.4 μM	4.9	>1000	48.24 ± 0.02	[b]
12	2.97	340	> 1 μM	-	>1000	11.41± 0.04	[b]
13	3.46	16 ± 1.8	5.8 μM	363	39 ± 2.1	42.30 ± 0.21	[b]
14	4.09	11 ± 2.2	24 μM	218	198	64.10 ± 5.58	22.02 ± 9.12
15	2.75	211	6.2 μM	29.4	>1000	85.50 ± 0.02	18.55 ± 7.72
16	2.61	167	3.9 μM	23.4	>1000	55.04 ± 6.69	[b]
17	4.80	171	749	4.4	>1000	[a]	[a]
18	5.30	7.9 ± 0.9	2.1 μM	256	1.7 μM	42.07 ± 0.04	[b]
19	4.35	2.2 ± 0.7	178 ± 12	81	>1000	45.20 ± 7.07	[b]
20	4.18	15 ± 1.1	462	30.8	>1000	64.80 ± 0.35	13.08 ± 6.31
21	5.48	606	>1 μM	-	>1000	10.75 ± 0.01	[b]
22	5.94	301	>1 μM	-	>1000	59.70 ± 2.24	[b]
23	5.28	9.0 ± 0.7	>1 μM	-	>1000	24.62 ± 0.05	[b]
24	4.91	2.9 ± 0.3	>1 μM	-	723	12.20 ± 1.72	[b]
25	3.17	9.0 ± 0.5	47 ± 2	5.2	39 ± 1.1	74.80 ± 3.56	13.07 ± 2.10
26	3.79	31 ± 4.2	111 ± 8	6.8	96 ± 2.7	80.01 ± 0.02	12.80 ± 1.79
27	3.74	17 ± 2.2	43 ± 1.9	2.5	49 ± 1.8	71.80 ± 1.60	7.64 ± 2.07
28	2.50	24 ± 3.4	58 ± 2.3	2.4	26 ± 0.9	[a]	[a]

29	2.73	68 ± 1.7	107 ± 10	1.6	20 ± 0.7	92.60 ± 0.03	4.28 ± 0.23
30	2.32	135 ± 11	704	5.2	96 ± 2.6	84.10 ± 0.02	13.94 ± 2.15
RRC-33	2.57	1.8 ± 0.1	45 ± 16	25	>1000	4.82 ± 2.15	[a]
Donepezil	4.41	14.6[c]	-	-	-	99.4 ± 0.01	0.012 ± 0.01
Ifenprodil	-	125 ± 24	98 ± 34	0.8	10 ± 0.7	-	-

Values are expressed as mean ± SEM of three experiments. Compounds with high affinity were tested three times. For compounds with low SR and NMDA affinity (> 150 nM), only one measure was performed.
[a] Compounds were not evaluated for solubility issues.
[b] Inhibition % < 60% at a concentration of 50 μM.
[c] Data taken from [38]

2.4 Molecular dynamic simulations and docking studies

Root mean square deviation (RMSD) values of S1R entire trimeric complex, monomer and binding pocket indicate that the protein structure is stable during MD simulations (RMSD of Cα atoms below 2 Å). The S1R structure in complex with 4-IBP was stable and no conformational changes occurred. The ligand formed H-bonds with the E172 for almost the entire simulation time (above 92%) but only in two binding pockets. In the third one, instead, the interaction was replaced by H-bonds with water molecules. The most representative cluster (occurring 41% of the simulation time) slightly differs from the others (average distance of 1.11 Å). However, the second cluster has also occurrence of 35% and the RMSD between them is 1.34 Å. They differ from the starting coordinates of 1.53 and 1.56 Å, respectively.

The most representative cluster was used to dock known (training set) and new (test set) S1R ligands. In particular, the best docking results were obtained with rigid docking without any constraints (AUC 0.78). However, not all active compounds were docked to the binding pocket: 4 out of 32 agonists were not successful, probably because they bind to a different conformation of the receptor. Indeed, results did not improve by flexible docking (AUC 0.53), and there is no crystal structure of the receptor in the active state that could be used to specifically investigate agonists.

Nevertheless, all active agonists formed ionic interactions with E172 and D126 due to their positively charged amine group. By contrast, low-ranked ligands lacked of these key residue contacts. Moreover, further amino acids (W89 and F107) were often involved in protein-ligand interactions: for instance, these residues were close to the protonated amine and eventually formed π-cation interactions. Furthermore, Y120 and H154 can form π-π stacking with ligand aromatic rings.

The docking pose of RRC-33 shows that the positively charged nitrogen atom forms ionic interactions with E172 and D126, and cation-π interactions with F107 (Figure 3). Moreover, hydrophobic contacts (not displayed) occur between the aromatic rings and surrounding amino acids (M93, L95, L105). The test set of new derivatives (**7-30**) was docked and all molecules conserved key interactions with the receptor as for the training set. Nevertheless, larger molecules with four rings (such as 4-biphenyl derivatives **12**, **16** and **30**) did not fit well into the binding pocket in comparison with smaller compounds. Indeed, either the biphenyl moiety clashed with Y206 or the benzyl ring did not have enough space on the opposite side of the pocket. In contrast, molecules **17**, **21** and **22** that have only two rings lacked important hydrophobic contacts resulting in low binding affinity. In conclusion, compounds with three rings, which conserved H-bond and hydrophobic interactions, seem to be the most interesting ones. In Figure 3, compounds **10** and **20** are reported by way of example.

All new derivatives were docked also to AChE. Flexible docking on AChE X-ray structure, both including and excluding water molecules, gave the best results. AUC was 0.71 in both cases, indicating that the model was able to distinguish between active compounds and decoys. The top-ranked ligands formed π-π and π-cation interactions with W86, W286, Y337 and Y341 residues of the binding pocket, as in the donepezil-bound crystal structure (Figure 3). Also, the H-bond with the backbone of F295 was mostly conserved. In particular, the presence of the carbonyl enhanced the binding when n was equal to 3 carbon atoms (compounds **25-30**), which is the optimal distance to keep the ionic interaction of the amine and the H-bond to F295. Instead, not all compounds formed

hydrogen bond interactions with the hydroxyl group of Tyr amino acids (compound **20**). For instance, the docking pose of compound **20** showed that the charged amine could fit into a deeper binding pocket, where it could form interactions with E202 (Figure 3). This was possible only for unsubstituted piperidine rings. Furthermore, the naphthalene ring (compounds **10** and **29**) enhanced the π-π stacking with W286.

In summary, docking poses suggested that the charged amine plays a key role not only for binding to negatively charged amino acids, but also to aromatic residues through cation-π interactions. The binding is strengthened by the presence of aromatic rings, which form hydrophobic and π-π interactions with both S1R and AChE ligand pockets. Several compounds among our new set of derivatives showed protein-ligand interaction patterns which are similar to reference compounds RRC-33 and donepezil, as shown in Figure 3, where the docking poses of **10** and **20** are reported.

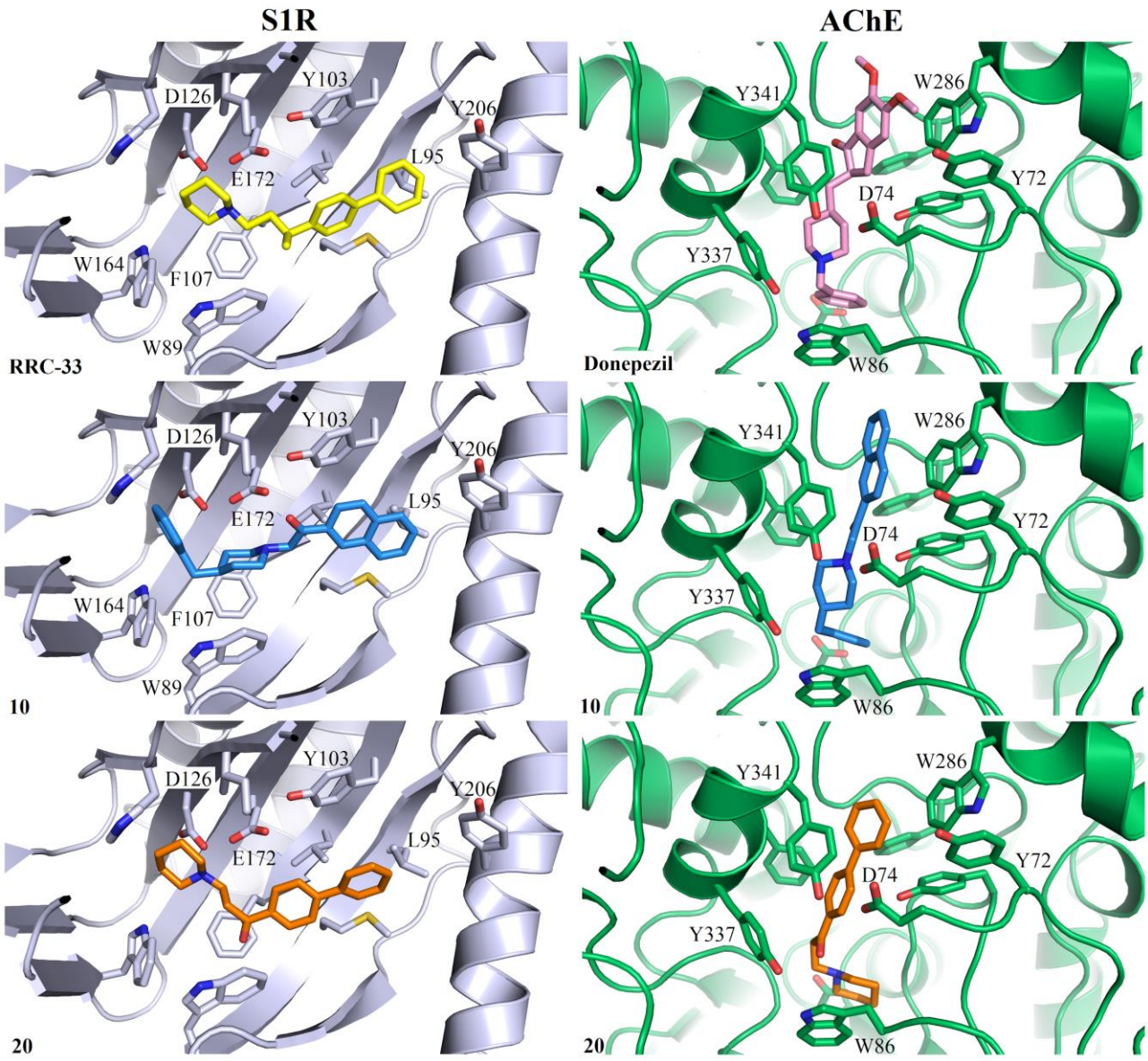

Figure 3. Docking poses of reference compounds (RRC-33 and donepezil) and of **10** and **20** on S1R (on the left side) and AChE (on the right side) binding pockets. Hydrogen atoms are not displayed. Ligands and key residues are shown as sticks.

2.5. Antioxidant profile and neurotrophic activity

Basing on preliminary biological investigations compounds **8**, **10**, **13-14**, **18-20**, **23-28** with either S1R affinity or both good S1R affinity and relevant AChE inhibitory activity were selected for further evaluations.

2.5.1. Free Radical Scavenging (FRS) activity

FRS activity of **8**, **10**, **13-14**, **18-20**, **23-28** was determined by 2,2-diphenyl-1-picrylhydrazyl (DPPH) assay, and the results were compared to those of reference molecules RRC-33, Donepezil and Cur. Stock solutions in EtOH of the tested compounds were prepared (5.0 mM). The DPPH absorbance was spectrophotometrically monitored at 515 nm and at a concentration of 465 μM; inhibition percentages are reported in Table SI2. These preliminary results demonstrated that compounds **13-14**, **18-20**, **23-28**, as well as RRC-33 and Donepezil do not display significant antioxidant activity (values ranging from 2.8% up to 32%). Conversely, compounds **8** and **10** could be considered promising antioxidant molecules, since they show an FRS activity (> 65%), comparable with the widely recognised Cur antioxidant activity. Accordingly, only molecules belonging to the n = 1 series possess intrinsic antioxidant properties, probably due to the higher radical delocalization, which generates stable derivatives. In the light of these data, the IC_{50} calculation of **8** and **10** was performed at four different concentrations (ranging from 465 to 45 μM).

*2.5.2 Cell viability and 2',7'-dichlorofluorescein diacetate (DCFDA) assay*s.

Toxicity of **8**, **10**, **13-14**, **18-20**, **23-28** was assessed in SH-SY5Y neuronal cell line, at different concentrations, ranging from 10 to 50 μM. The cell viability was evaluated through 3-(4,5-dimethylthiazol-2-yl)-5-(3-carboxymethoxyphenyl)-2-(4-sulfophenyl)-2H-tetrazolium (MTS) assay, after exposing cells to these compounds for 24 h and 48 h. The results are reported in Table 2. The tested compounds show a dose-dependent effect on SH-SY5Y cell lines (Homo Sapiens bone marrow

neuroblastoma) at different exposure times. Moreover, these values show that almost all molecules do not exhibit cytotoxic activities, with the exception of compound **23**, which decreases cell viability even at a 10 μM concentration (77%). We speculated that this countertrend could be due to the presence of morpholine as aminic moiety. Furthermore, compounds belonging to the n = 2 series and presenting a piperidine portion show cytotoxic properties when they are administered for 48 h at a concentration of 25 μM and 50 μM. Noteworthy, molecules with a 9-atoms linker between the two aromatic portions do not alter the cell viability even if they are employed at high doses. Lastly, for comparative purpose, RRC-33, Donepezil and Cur were subjected to MTS test. Also in this case, the results indicate the lack of toxicity. Considering the results obtained so far (good BBB score, good S1R affinity, high AChE inhibition percentage) compounds **10**, **14** and **20** were selected for a second screening aimed at calculating the IC_{50} value, by testing them at 6 different concentrations (ranging from 1 μM to 100 μM) for 24 and 48 h. Compounds **10** and **20** showed an IC_{50} higher than 20 μM (24 h = 52 and 37, respectively; 48 h = 57 and 22, respectively). The viability trend is reported in Figure 4.

Table 2. Viability test at 24 h and 48 h.

Cmpd	24 h			48 h		
	10 µM (%)	**25 µM (%)**	**50 µM (%)**	**10 µM (%)**	**25 µM (%)**	**50 µM (%)**
8	103 ± 0.03	98.4 ± 0.05	87 ± 0.03	85.5 ± 0.12	69.3 ± 0.03	52.5 ± 0.02
10	107 ± 0.05	104.2 ± 0.04	81.3 ± 0.03	89.5 ± 0.02	77.6 ± 0.04	48.4 ± 0.01
13	93 ± 0.01	48 ± 0.01	49 ± 0.01	106 ± 0.17	44 ± 0.04	36 ± 0.04
14	99.9 ± 0.01	63.9 ± 0.04	56.5 ± 0.05	97.4 ± 0.02	50.2 ± 0.05	44.7 ± 0.01
18	119 ± 0.02	86 ± 0.03	63 ± 0.01	104 ± 0.08	49.4 ± 0.06	43.4 ± 0.01
19	98.6 ± 0.04	66.4 ± 0.01	65.4 ± 0.01	70.3 ± 0.02	42 ± 0.01	40 ± 0.03
20	104 ± 0.06	95.4 ± 0.01	64 ± 0.05	95.9 ± 0.03	49.3 ± 0.04	44.7 ± 0.03
23	77 ± 0.04	48 ± 0.01	49 ± 0.01	79 ± 0.04	38 ± 0.06	37 ± 0.04
24	100 ± 0.01	73 ± 0.01	83.3 ± 0.08	100 ± 0.06	66 ± 0.03	62.4 ± 0.01
25	100 ± 0.04	100 ± 0.02	87 ± 0.01	96 ± 0.02	95 ± 0.05	54 ± 0.02
26	100 ± 0.01	100 ± 0.04	84.4 ± 0.01	97.3 ± 0.02	87 ± 0.04	61 ± 0.01
27	100 ± 0.03	100 ± 0.01	98 ± 0.01	94.8 ± 0.05	85.6 ± 0.03	65 ± 0.01
28	80.2 ± 0.04	86 ± 0.01	86 ± 0.07	77 ± 0.01	57 ± 0.01	61 ± 0.01
RRC-33	100 ± 0.03	100 ± 0.03	86 ± 0.04	84 ± 0.01	77.1 ± 0.01	57.3 ± 0.01
Donepezil	100 ± 0.01	99.3 ± 0.02	94.7 ± 0.01	94.3 ± 0.01	80.4 ± 0.01	64.4 ± 0.02
Curcumin	100 ± 0.01	76.5 ± 0.01	71.5 ± 0.01	100 ± 0.01	58.7 ± 0.01	59 ± 0.02

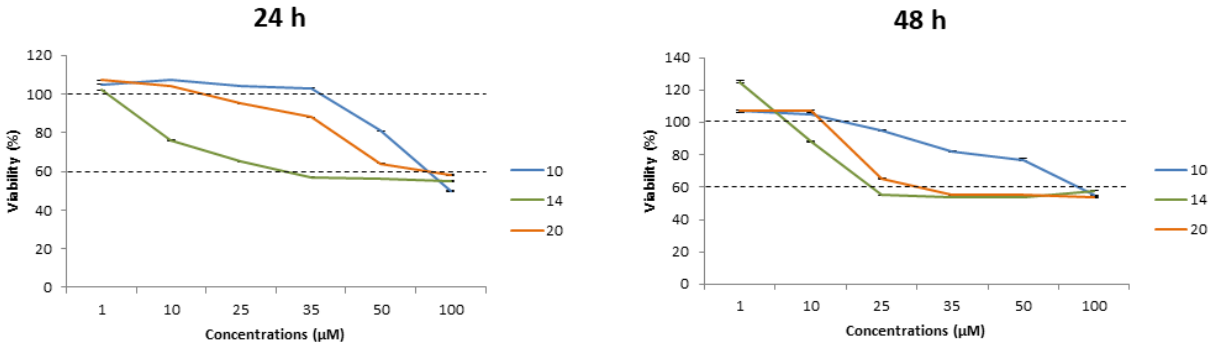

Figure 4. Viability trends of compounds **10**, **14** and **20**, after 24 and 48 h of exposure.

The major intracellular ROS sources are complex I (NADH dehydrogenase ubiquinone-ubiquinone reductase) and complex III (ubiquinone cytochrome C reductase), both of them take part to the mitochondrial electron transport chain [39]. A low ROS level plays a crucial role in cellular pathways. Nevertheless, when the ROS concentration increases and overcomes the cellular antioxidant machinery, it can induce macromolecular damages (*i.e.* interaction with the DNA, proteins and lipids) and compromise the thiol redox circuits, promoting aberrant molecular cascades [40]. Considering that oxidative stress, induced by the increase of ROS intracellular concentration, is a driving issue in neurodegenerative diseases, we evaluated the ability of **10**, **14** and **20** and reference compounds in reducing ROS within SH-SY5Y cells, after an exposure to oxidative damages mediated by H_2O_2. The assay provided the employment of DCFDA reagent, which diffuses within the cell and undergoes esterase-mediated de-acethylation. The so-obtained product is then subjected to oxidation by ROS, giving access to 2',7'-dichlorofluorescein, a high fluorescent molecule with adsorption and emission wavelength of 495 and 529 nm, respectively.

The compounds were tested at a concentration of 10 μM in the presence of H_2O_2 (180 μM) for 24 h. In parallel experiments, we evaluated the cell viability by MTS assay, to verify the lack of cytotoxicity under the same experimental conditions (Figure 5). The results reveal that all compounds show a safe profile and thus they can be evaluated through fluorescent assay. As reported in Figure 5, Cur possesses the ability to reduce ROS up to a 0%, whereas Donepezil and RRC-33 show no antioxidant properties. On the basis of our data, **10** and **20** are able to promote ROS reduction up to 43% and 18% respectively and thus can be considered antioxidant molecules, whereas **14** resulted ineffective and it was abandoned.

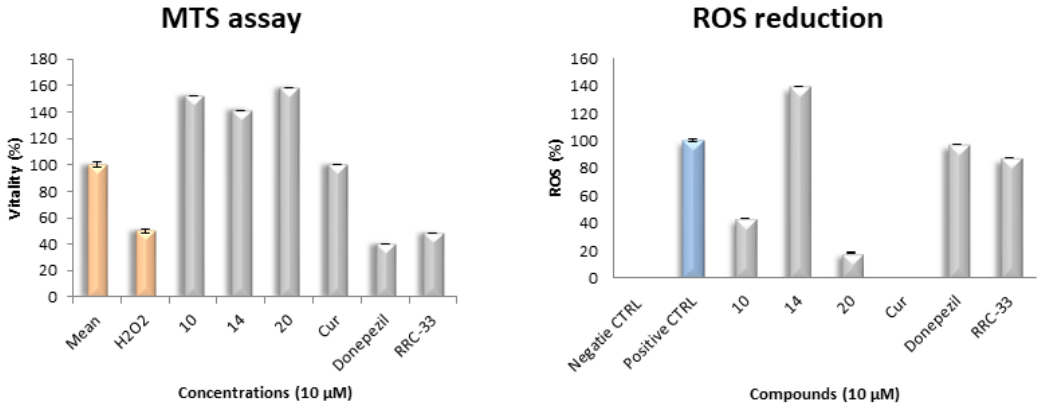

Figure 5. ROS percentage evaluation after administration of compounds **10**, **14**, **20**, Cur, Donepezil and (R)-RC-33.

2.5.4. Neurotrophic activity

Basing on our previous experience, we evaluated the neurotrophic effect of the most interesting compounds **10** and **20**, evaluating the neurite differentiation and elongation by using the straightforward model of Dorsal Root Ganglia (DRG) [16]. Briefly, DRG explants from E15 Sprague – Dawley rat embryos are able to sprout neurites when cultured with pro-differentiation agents, such as Nerve Growth Factor (NGF). The neurite elongation is promoted by neurotrophic drugs and blocked or slowed up by neurotoxic agents. Compounds **10** and **20** were tested at different concentration, after 24 and 48 hours of exposure (Figure 6 and Figures SI1-SI4). Interestingly, both compounds showed neurotrophic effect. In particular, best results were obtained for compound **10** at the concentration of 2.5µM, starting from 24 hours of exposure and leading to an increase of the neurite length of about 15% with respect to the untreated control DRG. For compound **20,** the concentrations 5µM and 2.5µM resulted to be the most effective, both after 24 hours and after 48 hours of exposure, with an increase of neurite length of about 20% with respect to control DRG. For both compounds, none concentrations resulted neurotoxic, except at the concentration 10µM, which showed after 24 hours of exposure an only transient neurotoxic effect, being disappeared after 48

hours. The present results demonstrated the pro-differentiation properties of compounds **10** and **20**, thus confirming their neurotrophic effect.

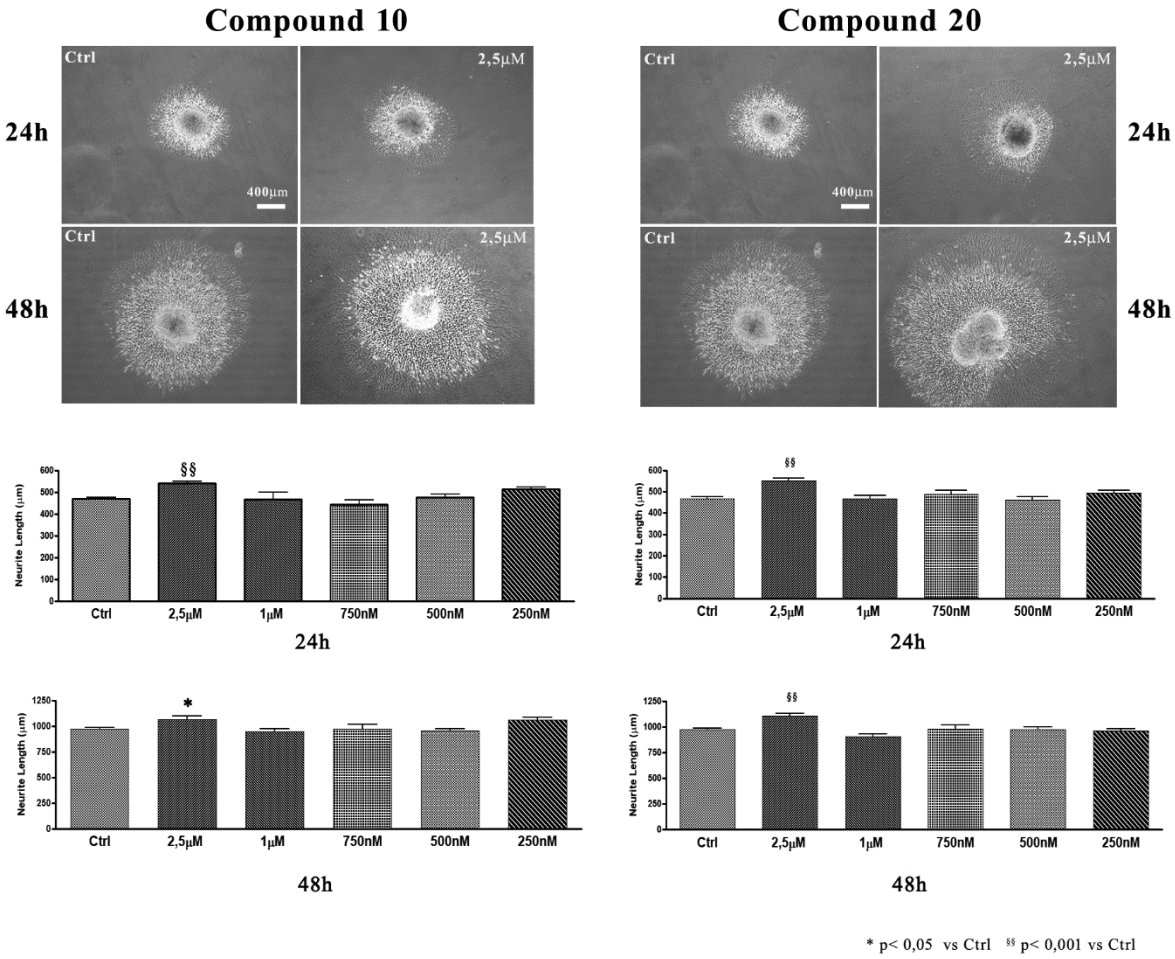

Figure 6. Evaluation of Neurotrophic activity of compounds **10** and **20**, after 24h and 48h of exposure.

3. Conclusion

In the present paper we discovered dual S1R modulators/AChE inhibitors endowed with antioxidant and neurotrophic properties. The adopted medicinal chemistry approach led to a novel series of compounds sharing the pharmacophoric requirements for interacting with both S1R and AChE, as confirmed by the molecular modelling study. Within the whole series, three compounds resulted endowed with considerable S1R affinity, good selectivity over S2R and AChE inhibition activity.

Their effect on neuroblastoma cell (SH-SY5Y) survival was evaluated and the ROS damage was mimicked by exposing SH-SY5Y cells to H_2O_2. The results highlighted that only compounds **10** and **20** decrease ROS production, thus ameliorating the cellular survival and therefore, they were selected for further experimental investigations. To this purpose, their effect on neurite outgrowth in DRG in vitro model was assessed and their neurotrophic role confirmed. Of note, the tested compounds did not show any cytotoxic effect at the concentration assayed.

Overall, our *hit* compounds **10** and **20** combine in the same molecule the S1R modulation and the AchE inhibition, together with cell damage protection and neurotrophic properties. Both compounds will undergo a structure optimization program for the development of therapeutic candidates for neurodegenerative diseases treatment.

4. Materials and Methods

4.1. General remarks

Reagents and solvents for synthesis were obtained from Aldrich (Italy). Solvents were purified according to the guidelines in Purification of Laboratory Chemicals. Thermal characterization was performed by using differential scanning calorimetry (DSC) and thermogravimetric analysis (TGA) on a Mettler Star^e System equipped with a DSC 821^e and TGA-DSC1 cell, respectively. Samples were weighed and placed in sealed aluminum (DSC) or alumina (TGA) pans. The samples were heated from 30 °C to 300 °C with a scanning rate of 10 °C/min under nitrogen atmosphere. The instruments were previously calibrated with Indium as standard reference. For FT-IR analysis a Spectrum One Perkin Elmer spectrophotometer equipped with a MIRacle™ ATR device was used. The IR spectra were scanned over wavenumber range of 4000-650 cm^{-1} with a resolution of 4 cm^{-1}. Analytical thin-layer-chromatography (TLC) was carried out on silica gel precoated glass-backed plates (Fluka Kieselgel 60 F254, Merck); visualized by ultra-violet (UV) radiation, acidic ammonium molybdate (IV), or potassium permanganate. Flash chromatography (FC) was performed with Silica

Gel 60 (particle size 230–400 mesh, purchased from Sigma Aldrich). Proton nuclear magnetic resonance (NMR) spectra were recorded on a Bruker Avance 500, 400 and 200 spectrometers operating at 500 MHz, 400 MHz and 200 MHz, respectively. Proton chemical shifts (δ) are reported in ppm with the solvent reference relative to tetramethylsilane (TMS) employed as the internal standard ($CDCl_3$, δ = 7.26 ppm). The following abbreviations are used to describe spin multiplicity: s = singlet, d = doublet, t = triplet, q = quartet, m = multiplet, br = broad signal, dd = doublet-doublet, td = triplet-doublet. The coupling constant values are reported in Hz. ^{13}C NMR spectra were recorded on a 500 MHz and 400 MHz spectrometers operating at 125 MHz, 100 MHz and 50 MHz, respectively, with complete proton decoupling. Carbon chemical shifts (δ) are reported in ppm relative to TMS with the respective solvent resonance as the internal standard ($CDCl_3$, δ = 77.23 ppm).

UPLC-UV-ESI/MS analyses were carried out on a Acuity UPLC Waters LCQ FLEET system using an ESI source operating in positive ion mode, controlled by ACQUIDITY PDA and 4 MICRO (Waters). Analyses were run on a ACQUITY BEH Phenyl (ABP) (50 x 2.1 mm, 1.7 μm) or ACQUITY BEH Shield (ABS) (100 x 2.1 mm, 1.7 μm) columns, at room temperature, with gradient elution (solvent A: water containing 0.1% of formic acid; solvent B: methanol containing 0.1% of formic acid; gradient: 10% B in A to 100% B in 3 minutes, followed by isocratic elution 100% B for 1.5 minutes, return to the initial conditions in 0.2 minutes) at a flow rate of 0.5 mL min-1. All of the final compounds had 95% or greater purity.

4.2. General procedure for the preparation of compounds 2-3

To an aqueous solution of K_2CO_3 (2.0 equiv.) was added Et_2O and *N,O*-dimethylhydroxyamine hydrochloride (1.5 equiv.). The resulting mixture was cooled at 0 °C and after 2 minutes the corresponding acyl chloride (1.0 equiv.) was added dropwise. The reaction was stirred overnight until

the room temperature was reached. The reaction mixture was extracted with Et_2O (2 x 5 mL) and washed with water (5 mL) and brine (10 mL). The organic phase was dried (anhydrous Na_2SO_4), filtered and, after removal of the solvent under reduced pressure, the pure compounds **2-3** were obtained.

3-chloro-N-methoxy-N-methylpropanamide (**2**) By following the General Procedure, starting from 3-chloropropanoyl chloride (127 mg, 1.00 mmol, 1.0 equiv), K_2CO_3 (276 mg, 2.0 mmol, 2.0 equiv), N,O-dimethylhydroxyamine hydrochloride (146 mg, 1.5 mmol, 1.5 equiv), H_2O (3 mL) and Et_2O (3 mL), the desired product was obtained in a quantitative amount (> 99.9 %) (151 mg) as a bright yellow oil. ^{1}H NMR (500 MHz, $CDCl_3$) δ: 3.80 (t, *J* = 6.9 Hz, 2H, CH_2CH_2Cl), 3.70 (s, 3H, $NOCH_3$), 3.19 (s, 3H, NCH_3), 2.91 (t, *J* = 6.7 Hz, 2H, CH_2CH_2CO). ^{13}C NMR (125 MHz, $CDCl_3$) δ: 170.8, 61.4, 39.2, 35.0, 32.0.

4-chloro-N-methoxy-N-methylbutanamide (**3**) By following the General Procedure, starting from 4-chlorobutanoyl chloride (141 mg, 1.00 mmol, 1.0 equiv), K_2CO_3 (276 mg, 2.0 mmol, 2.0 equiv), N,O-dimethylhydroxyamine hydrochloride (146 mg, 1.5 mmol, 1.5 equiv), H_2O (3 mL) and Et_2O (3 mL), the desired product was obtained in 92% (152 mg) as a bright yellow oil. ^{1}H NMR (500 MHz, $CDCl_3$) δ: 3.70 (s, 3H, $NOCH_3$), 3.63 (t, *J* = 6.4 Hz, 2H, CH_2CH_2Cl), 3.18 (s, 3H, NCH_3), 2.62 (t, *J* = 6.7 Hz, 2H, CH_2CH_2CO), 2.11 (m, *J* = 6.9 Hz, 2H, $CH_2CH_2CH_2$). ^{13}C NMR (125 MHz, $CDCl_3$) δ: 173.3, 61.3, 44.7 32.1, 28.6, 27.1.

4.3. General procedure for the preparation of compounds 4a, 5a-c and 6a

To a solution of Weinreb amide (1.0 equiv.) in ACN, the corresponding amine (1.0 equiv.) and K_2CO_3 (1.5 equiv.) were added. The mixture was stirred overnight, at room temperature. After removal of the solvent under reduced pressure, the crude was extracted with DCM (3 x 5 mL) and washed with

water (5 mL) and brine (10 mL). In the case of compound **4a**, this work-up was sufficient to obtain the pure compound. Conversely, an acid (pH = 3-4) / base (pH = 8-9) work-up was required for **5a-c** and **6a**, the combined organic phases were dried (anhydrous Na_2SO_4), filtered and, evaporated under vacuum to get the desired compounds. The crude compound **6a** was further purified through flash chromatography (silica gel) to afford pure compound **6a**.

2-(4-benzylpiperidin-1-yl)-N-methoxy-N-methylacetamide (**4a**) By following the General Procedure, starting from 2-chloro-*N*-methoxy-*N*-methylacetamide (138 mg, 1.00 mmol, 1.0 equiv), K_2CO_3 (207 mg, 1.5 mmol, 1.5 equiv), 4-benzylpiperidine (175 mg, 176 mL 1.0 mmol, 1.0 equiv) and ACN (7 mL), the desired product was obtained in quantitative amount (276 mg) as a bright yellow oil. ^{1}H NMR (500 MHz, $CDCl_3$) δ: 7.27 (m, 2H, Ar), 7.18 (t, 1H, *J* = 7.5 Hz, Ar), 7.14 (d, 2H, *J* = 7.3 Hz, Ar), 3.69 (s, 3H, NOC*H*$_3$), 3.29 (s, 2H, C*H*$_2$N), 3.16 (s, 3H, NC*H*$_3$), 2.96 (d, 2H, Pip-2, Pip-6), 2.53 (d, 2H, C*H*$_2$Pip-4), 2.07 (t, 2H, Pip-2, Pip-6), 1.62 (d, 2H, Pip-3, Pip-5), 1.51 (m, 1H, Pip-4), 1.40 (q, 2H, Pip-3, Pip-5). ^{13}C NMR (125 MHz, $CDCl_3$) δ: 171.4, 140.5, 129.1, 128.1, 125.7, 61.3, 58.5, 54.1, 43.1, 37.5, 32.1, 32.0.

3-(4-benzylpiperidin-1-yl)-N-methoxy-N-methylpropanamide (**5a**) By following the General Procedure, starting from 3-chloro-*N*-methoxy-*N*-methylpropanamide (152 mg, 1.00 mmol, 1.0 equiv), K_2CO_3 (207 mg, 1.5 mmol, 1.5 equiv), 4-benzylpiperidine (175 mg, 176 mL, 1.0 mmol, 1.0 equiv) and ACN (7 mL), the desired product was obtained in quantitative amount (290 mg) as a bright yellow oil. ^{1}H NMR (500 MHz, $CDCl_3$) δ: 7.27 (m, 2H, Ar), 7.18 (t, 1H, *J* = 7.4 Hz, Ar), 7.13 (d, 2H, *J* = 7.4 Hz, Ar), 3.68 (s, 3H, NOC*H*$_3$), 3.16 (s, 3H, NC*H*$_3$), 2.95 (d, 2H, Pip-2, Pip-6), 2.72-2.70 (m, 4H, C*H*$_2$N, C*H*$_2$CH$_2$N), 2.53 (d, 2H, C*H*$_2$Pip-4), 2.00 (t, 2H, Pip-2, Pip-6), 1.65 (d, 2H, Pip-3, Pip-5),

1.54 (m, 1H, Pip-4), 1.36 (q, 2H, Pip-3, Pip-5). ^{13}C NMR (125 MHz, $CDCl_3$) δ: 173.1, 140.5, 129.1, 128.1, 125.8, 61.3, 53.8, 53.6, 43.0, 37.6, 37.1, 32.1, 29.5.

N-methoxy-N-methyl-3-(piperidin-1-yl)propanamide (**5b**) By following the General Procedure, starting from 3-chloro-*N*-methoxy-*N*-methylpropanamide (152 mg, 1.00 mmol, 1.0 equiv), K_2CO_3 (207 mg, 1.5 mmol, 1.5 equiv), piperidine (85 mg, 99 mL, 1.0 mmol, 1.0 equiv) and ACN (7 mL), the desired product was obtained in quantitative amount (200 mg) as a bright yellow oil. ^{1}H NMR (400 MHz, $CDCl_3$) δ: 3.76 (s, 3H, NOC*H*$_3$), 3.24 (s, 3H, NC*H*$_3$), 2.76 (s, 4H, C*H*$_2$N, C*H*$_2$CH$_2$N), 2.52 (t, 4H, Pip-2, Pip-6), 1.70-1.56 (m, 6H, Pip-3, Pip-4, Pip-5). ^{13}C NMR (100 MHz, $CDCl_3$) δ: 175.2, 61.3, 54.5, 54.2, 29.7, 25.9, 24.2.

N-methoxy-N-methyl-3-morpholinopropanamide (**5c**) By following the General Procedure, starting from 3-chloro-*N*-methoxy-*N*-methylpropanamide (152 mg, 1.00 mmol, 1.0 equiv), K_2CO_3 (207 mg, 1.5 mmol, 1.5 equiv), morpholine (87 mg, 87 mL, 1.0 mmol, 1.0 equiv) and ACN (7 mL), the desired product was obtained in 46 % (93 mg) as a bright yellow oil. ^{1}H NMR (400 MHz, $CDCl_3$) δ: 3.78-3.73 (m, 4H, NCH$_2$C*H*$_2$O), 3.73 (s, 3H, NOC*H*$_3$), 3.22 (s, 3H, NC*H*$_3$), 2.81-2.63 (m, 4H, CH$_2$C*H*$_2$N, C*H*$_2$CH$_2$N), 2.56-2.51 (t, 4H, NC*H*$_2$CH$_2$O). ^{13}C NMR (100 MHz, $CDCl_3$) δ: 175.3, 66.9, 61.3, 53.9, 53.6, 32.2, 29.4.

4-(4-benzylpiperidin-1-yl)-N-methoxy-N-methylbutanamide (**6a**) By following the General Procedure, starting from 4-chloro-*N*-methoxy-*N*-methylbutanamide (166 mg, 1.00 mmol, 1.0 equiv), K_2CO_3 (207 mg, 1.5 mmol, 1.5 equiv), 4-benzylpiperidine (175 mg, 176 mL 1.0 mmol, 1.0 equiv) and ACN (7 mL), the desired product was obtained in 65 % (198 mg) as a bright yellow oil after chromatography on silica gel (60:40 ethylacetate:*n*-hexane). ^{1}H NMR (400 MHz, $CDCl_3$) δ: 7.33-

7.12 (m, 5H, Ar), 3.69 (s, 3H, NOCH_3), 3.48 (s, 2H, CH_2N), 3.18 (s, 3H, NCH_3), 2.74-2.66 (m, 2H, Pip-2, Pip-6), 2.60-2.50 (m, 4H, CH_2Pip-4, Pip-2, Pip-6), 2.31-2.21 (m, COCH_2CH$_2$), 2.09-1.94 (m, 2H, COCH$_2$CH_2CH$_2$), 1.82-1.65 (m, 5H, Pip-3, Pip-4, Pip-5). ^{13}C NMR (125 MHz, $CDCl_3$) δ: 173.6, 139.9, 129.1, 128.3, 126.1, 61.1, 57.1, 53.1, 42.5, 37.2, 30.3, 29.5, 20.3.

4.4. General procedure for the preparation of compounds 7-30

Under argon atmosphere, *tert*-butyllithium (2.2 equiv., 1.9 M in pentane) was added dropwise to a -78 °C cooled solution of the appropriate arylbromide (1.5 equiv.) in anhydrous THF. After 20 minutes, the solution of the corresponding Weinreb amide in anhydrous THF was added dropwise. The stirring was continued for 5 additional hours and then quenched with water. The reaction was extracted with Et_2O (2 x 5 mL) and washed with water (5 mL) and brine (10 mL). The organic phase was dried (anhydrous Na_2SO_4), filtered and, after removal of the solvent under reduced pressure, the so-obtained crude mixture was subjected to chromatography (silica gel) to afford pure compounds. Lastly, pure compounds were converted into their corresponding hydrochlorides, adding an ethereal solution of HCl (1.0 equiv., 1 M in Et_2O).

4-benzyl-1-(2-oxo-2-phenylethyl)piperidin-1-ium hydrochloride (**7**) By following the General Procedure, starting from bromobenzene (236 mg, 1.5 mmol, 1.5 equiv.), 2-(4-benzylpiperidin-1-yl)-*N*-methoxy-*N*-methylacetamide (274 mg, 1.00 mmol, 1.0 equiv.), *t*-BuLi (1.9 M, 1.32 mL, 2.5 mmol, 2.5 equiv.) and THF (5 mL), the desired product was obtained in 40% (117 mg) as a bright yellow oil after chromatography on silica gel (60:40 hexane:etylacetate) and converted into the corresponding hydrochloride. FT-IR (cm^{-1}): 3058, 3023, 2922, 2846, overtones Ar = 2100-1800, 1706, 1598, 1580, 1448. ^{1}H NMR (400 MHz, $CDCl_3$) δ: 12.07 (s, 1H, NH^+), 7.95 (brs, 2H, Ar), 7.65 (brs, 1H, Ar), 7.50 (brs, 2H, Ar), 7.31 (t, *J* = 7.0 Hz, 2H, Ar), 7.23 (t, *J* = 8.0 Hz, 1H, Ar), 7.16 (d, *J* = 8.0 Hz, 2H, Ar),

4.75 (s, 2H, COC*H*$_2$N), 3.55 (brs, 4H, Pip-2, Pip-6), 2.64 (m, 2H, C*H*$_2$Pip-4), 2.09-1.85 (m, 5H, Pip-3, Pip-4, Pip-5). ^{13}C NMR (100 MHz, $CDCl_3$) δ: 190.3, 139.0, 134.9, 133.9, 129.1, 128.9, 128.4, 128.1, 126.3, 59.7, 52.4, 42.0, 35.9, 29.3. UHPLC-ESI-MS: ABS t_R = 1.19, 96% pure (λ = 210 nm), m/z = 294.3 $[M + H]^+$.

The thermal profile showed two endothermic effects; the first of little intensity at 136.9 ± 0.5 °C, not associated with a mass loss in TGA curve, was probably attributable to a metastable phase melting, followed by a recrystallization exotherm at around 142 °C and a second endothermic effect due to the melting at 208.4 ± 0.1 °C (ΔH_{fus} = 50 ± 1 Jg^{-1}).of a stable phase.

4-benzyl-1-(2-(4-methoxyphenyl)-2-oxoethyl)piperidin-1-ium hydrochloride (**8**) By following the General Procedure, starting from 1-bromo-4-methoxybenzene (281 mg, 1.5 mmol, 1.5 equiv.), 2-(4-benzylpiperidin-1-yl)-*N*-methoxy-*N*-methylacetamide (274 mg, 1.00 mmol, 1.0 equiv.), *t*-BuLi (1.9 M, 1.32 mL, 2.5 mmol, 2.5 equiv.) and THF (5 mL), the desired product was obtained in 37% (120 mg) as a bright yellow oil after chromatography on silica gel (60:40 hexane:etylacetate) and converted into the corresponding hydrochloride. FT-IR (cm^{-1}): 3059, 3013, 2932, overtones Ar = 2100-1750, 1694, 1603, 1578, 1512, 1402. ^{1}H NMR (400 MHz, $CDCl_3$) δ: 11.93 (brs, 1H, N*H*$^+$), 7.90 (d, *J* = 8.0 Hz, 2H, Ar), 7.30 (t, *J* = 8.0 Hz, 2H, Ar), 7.22 (t, *J* = 8.0 Hz, 1H, Ar), 7.15 (d, *J* = 8.0 Hz, 2H, Ar), 6.93 (d, *J* = 8.0 Hz, 2H, Ar), 4.68 (s, 2H, COC*H*$_2$N), 3.87 (s, 3H, OC*H*$_3$), 3.51 (brd, 4H, Pip-2, Pip-6), 2.63 (d, 2H, C*H*$_2$Pip-4), 2.06 (m, 2H, Pip-3, Pip-5), 1.85-1.82 (m, 3H, Pip-3, Pip-4, Pip-5). ^{13}C NMR (100 MHz, $CDCl_3$) δ: 188.5, 164.8, 148.5, 139.0, 130.5, 128.9, 128.4, 126.9, 126.2, 114.2, 59.1, 55.6, 52.2, 42.0, 35.8, 29.3. UHPLC-ESI-MS: ABP t_R = 1.87, 98% pure (λ = 210 nm), m/z = 324.4 $[M + H]^+$.

The thermal profile was typical of an anhydrous form showing the melting endothermic effect at 233.1 ± 0.7 °C (ΔH_{fus} = 136 ± 4 Jg^{-1}).

4-benzyl-1-(2-(3-methoxyphenyl)-2-oxoethyl)piperidin-1-ium hydrochloride (**9**) By following the General Procedure, starting from 1-bromo-3-methoxybenzene (281 mg, 1.5 mmol, 1.5 equiv.), 2-(4-benzylpiperidin-1-yl)-*N*-methoxy-*N*-methylacetamide (274 mg, 1.00 mmol, 1.0 equiv.), *t*-BuLi (1.9 M, 1.32 mL, 2.5 mmol, 2.5 equiv.) and THF (5 mL), the desired product was obtained in 48% (155 mg) as a bright yellow oil after chromatography on silica gel (60:40 hexane:etylacetate) and converted into the corresponding hydrochloride. FT-IR (cm^{-1}): 3056, 3026, 3003, 2923, 2841, overtones Ar = 2100-1750, 1696, 1596, 1431. ^{1}H NMR (400 MHz, $CDCl_3$) δ: 11.94 (brs, 1H, N*H*$^{+}$), 7.49-7.16 (m, 9H, Ar), 4.77 (s, 2H, COC*H*$_2$N), 3.84 (s, 3H, OC*H*$_3$), 3.56 (m, 4H, Pip-2, Pip-6), 2.63 (brd, 2H, C*H*$_2$Pip-4), 2.08 (brs, 2H, Pip-3, Pip-5), 1.86-1.73 (m, 3H, Pip-3, Pip-4, Pip-5). ^{13}C NMR (100 MHz, $CDCl_3$) δ:190.1, 160.0, 139.0, 135.2, 130.1, 128.9, 128.4, 126.3, 121.4, 120.6, 112.2, 60.0, 55.6, 52.5, 42.0, 35.8, 29.3. UHPLC-ESI-MS: ABP t_R = 1.85, 99% pure (λ = 220 nm), m/z = 324.4 $[M + H]^+$. The thermal profile showed a first broad endothermic effect at 147.2 ± 0.7 °C followed by melting at 191.4 ± 0.5 °C (ΔH_{fus} = 61 ± 5 Jg^{-1}). The first endothermic effect, not associated with a mass loss in TGA curve, was probably attributable to the melting of a metastable phase.

4-benzyl-1-(2-(naphthalen-2-yl)-2-oxoethyl)piperidin-1-ium hydrochloride (**10**) By following the General Procedure, starting from 2-bromonaphthalene (311 mg, 1.5 mmol, 1.5 equiv.), 2-(4-benzylpiperidin-1-yl)-*N*-methoxy-*N*-methylacetamide (274 mg, 1.00 mmol, 1.0 equiv.), *t*-BuLi (1.9 M, 1.32 mL, 2.5 mmol, 2.5 equiv.) and THF (5 mL), the desired product was obtained in 54% (185 mg) as a bright yellow oil after chromatography on silica gel (60:40 hexane:etylacetate) and converted into the corresponding hydrochloride. FT-IR (cm^{-1}): 3023, 2924, overtones Ar = 2100-1800, 1689, 1599, 1495, 1453. ^{1}H NMR (400 MHz, $CDCl_3$) δ: 11.63 (brs, 1H, N*H*$^{+}$), 8.51 (s, 1H, Nap), 7.91 (d, 2H, Nap), 7.78 (t, 2H, Nap), 7.59 (t, *J* = 8.0 Hz, 1H, Nap), 7.51 (t, *J* = 8.0 Hz, 1H, Nap), 7.28-7.11 (m, 5H, Ar), 4.96 (s, 2H, COC*H*$_2$N), 3.60-3.52 (m, 4H, Pip-2, Pip-6), 2.59 (brd, 2H, C*H*$_2$Pip-4), 2.04

(m, 2H, Pip-3, Pip-5), 1.82-1.79 (m, 3H, Pip-3, Pip-4, Pip-5). ^{13}C NMR (100 MHz, $CDCl_3$) δ:190.2, 139.0, 136.0, 132.0, 131.0, 130.7, 129.8, 129.4, 128.9, 128.4, 127.6, 127.2, 126.2, 122.6, 59.9, 52.7, 41.9, 35.7, 29.3. UHPLC-ESI-MS: ABP t_R = 2.08, 95% pure (λ = 210 nm), m/z = 344.3 $[M + H]^+$.

The thermal profile showed an exothermic effect at 191.9 ± 0.6 °C, probably due to the crystallization of an amorphous portion of sample, induced by heating. The melting of the anhydrous form was recorded at 212.0 ± 0.9 °C (ΔH_{fus} = 69 ± 5 Jg^{-1}).

4-benzyl-1-(2-(6-methoxynaphthalen-2-yl)-2-oxoethyl)piperidin-1-ium hydrochloride (**11**) By following the General Procedure, starting from 2-bromo-6-methoxynaphthalene (256 mg, 1.5 mmol, 1.5 equiv.), 2-(4-benzylpiperidin-1-yl)-*N*-methoxy-*N*-methylacetamide (274 mg, 1.00 mmol, 1.0 equiv.), *t*-BuLi (1.9 M, 1.32 mL, 2.5 mmol, 2.5 equiv.) and THF (5 mL), the desired product was obtained in 49% (183 mg) as a bright yellow oil after chromatography on silica gel (60:40 hexane:etylacetate) and converted into the corresponding hydrochloride. FT-IR (cm^{-1}): 3023, 2932, overtones Ar = 2100-1800, 1682, 1483. ^{1}H NMR (400 MHz, $CDCl_3$) δ: 11.46 (brs, 1H, N*H*$^+$), 8.38 (s, 1H, Nap), 7.79 (m, 2H, Nap), 7.61 (brd, 1H, Nap), 7.28-7.00 (m, 7H, Ar, Nap), 4.92 (s, 2H, COC*H*$_2$N), 3.90 (s, 3H, OC*H*$_3$), 3.59-3.53 (m, 4H, Pip-2, Pip-6), 2.58 (brd, 2H, C*H*$_2$Pip-4), 2.03 (m, 2H, Pip-3, Pip-5), 1.82-1.79 (m, 3H, Pip-3, Pip-4, Pip-5). ^{13}C NMR (100 MHz, $CDCl_3$) δ: 189.7, 160.4, 139.0, 137.9, 131.4, 130.5, 129.0, 128.9, 128.3, 127.5, 127.3, 126.2, 123.4, 120.1, 105.7, 59.9, 55.4, 52.7, 42.0, 35.7, 29.3. UHPLC-ESI-MS: ABS t_R = 1.63, 95% pure (λ = 210 nm), m/z = 374.5 $[M + H]^+$.

The thermal profile showed an exothermic effect at 137.9 ± 0.4 °C, attributable to crystallization, induced by heating, of an amorphous portion of sample,. The melting of the anhydrous crystalline form was recorded at 212.9 ± 0.9 °C (ΔH_{fus} = 50 ± 2 Jg^{-1}).

1-(2-([1,1'-biphenyl]-4-yl)-2-oxoethyl)-4-benzylpiperidin-1-ium hydrochloride (**12**) By following the General Procedure, starting from 4-bromo-1,1'-biphenyl (350 mg, 1.5 mmol, 1.5 equiv.), 2-(4-benzylpiperidin-1-yl)-*N*-methoxy-*N*-methylacetamide (274 mg, 1.00 mmol, 1.0 equiv.), *t*-BuLi (1.9 M, 1.32 mL, 2.5 mmol, 2.5 equiv.) and THF (5 mL), the desired product was obtained in 33% (122 mg) as a bright yellow oil after chromatography on silica gel (60:40 hexane:etylacetate) and converted into the corresponding hydrochloride. FT-IR (cm^{-1}): 3025, 2986, 2935, 2916, 2847, overtones Ar = 2100-1800, 1691, 1603, 1414. ^{1}H NMR (400 MHz, $CDCl_3$) δ: 11.70 (brs, 1H, N*H*$^{+}$), 8.00 (d, *J* = 6.3 Hz, 2H, Ar), 7.66 (brs, 2H, Ar), 7.55 (ds, *J* = 4.0 Hz, 2H, Ar), 7.44 (m, 3H, Ar), 7.28-7.13 (m, 5H, Ar), 4.88 (s, 2H, COC*H*$_2$N), 3.60-3.55 (m, 4H, Pip-2, Pip-6), 2.62-2.52 (brs, 2H, C*H*$_2$Pip-4), 2.07 (m, 2H, Pip-3, Pip-5), 1.86-1.83 (m, 3H, Pip-3, Pip-4, Pip-5). ^{13}C NMR (100 MHz, $CDCl_3$) δ: 189.8, 147.4, 139.0, 138.9, 132.5, 129.0, 128.7, 128.6, 128.4, 127.5, 127.1, 126.2, 60.0, 52.7, 42.0, 35.8, 29.3. UHPLC-ESI-MS: ABP t_R = 2.22, 98% pure (λ = 210 nm), m/z = 370.5 $[M + H]^+$.

The thermal profile was typical of an anhydrous form showing the melting endothermic effect at 208.2 ± 0.4 °C (ΔH_{fus} = 64 ± 2 Jg^{-1}).

3-(4-benzylpiperidin-1-yl)-1-phenylpropan-1-one (**13**) By following the General Procedure, starting from bromobenzene (236 mg, 1.5 mmol, 1.5 equiv.), 3-(4-benzylpiperidin-1-yl)-*N*-methoxy-*N*-methylpropanamide (290 mg, 1.00 mmol, 1.0 equiv.), *t*-BuLi (1.9 M, 1.32 mL, 2.5 mmol, 2.5 equiv.) and THF (5 mL), the desired product was obtained in 28% (86 mg) as a bright yellow oil after chromatography on silica gel (90:10 etylacetate:methanol) and converted into the corresponding hydrochloride. FT-IR (cm^{-1}): 3059, 3045, 3025, 2996, 2921, overtones Ar = 2100-1700, 1682, 1596, 1447. ^{1}H NMR (500 MHz, $CDCl_3$) δ: 7.88 (d, *J* = 8.3 Hz, 2H, Ar), 7.48 (m, 1H, Ar), 7.38 (t, *J* = 7.5 Hz, 2H, Ar), 7.20 (m, 2H, Ar), 7.11 (t, *J* = 7.0 Hz, 1H, Ar), 7.06 (d, *J* = 7.4 Hz, 2H, Ar), 3.17 (m, 2H, COC*H*$_2$CH$_2$), 2.91 (d, 2H, Pip-2, Pip-6), 2.77 (m, 2H, CH$_2$C*H*$_2$N), 2.47 (d, *J* = 7.2 Hz, 2H, C*H*$_2$Pip-

4), 1.96 (m, 2H, Pip-2, Pip-6), 1.59 (d, 2H, Pip-3, Pip-5), 1.48 (m, 1H, Pip-4), 1.30 (m, 2H, Pip-3, Pip-5). ^{13}C NMR (125 MHz, $CDCl_3$) δ: 199.0, 140.4, 136.7, 133.1, 129.0, 128.6, 128.1, 128.0, 125.8, 53.9, 53.3, 43.0, 37.6, 36.1, 31.8. UHPLC-ESI-MS: ABS t_R = 1.25, 95% pure (λ = 254 nm), m/z = 308.4 $[M + H]^+$.

The thermal profile was typical of an anhydrous form showing the melting endothermic effect at 193.4 ± 0.7 °C (ΔH_{fus} = 175 ± 2 Jg^{-1}).

3-(4-benzylpiperidin-1-yl)-1-(4-methoxyphenyl)propan-1-one (**14**) By following the General Procedure, starting from 1-bromo-4-methoxybenzene (281 mg, 1.5 mmol, 1.5 equiv.), 3-(4-benzylpiperidin-1-yl)-*N*-methoxy-*N*-methylpropanamide (290 mg, 1.00 mmol, 1.0 equiv.), *t*-BuLi (1.9 M, 1.32 mL, 2.5 mmol, 2.5 equiv.) and THF (5 mL), the desired product was obtained in 25% (84 mg) as a bright yellow oil after chromatography on silica gel (90:10 etylacetate:methanol) and converted into the corresponding hydrochloride. FT-IR (cm^{-1}): 3048, 3030, 3005, 2939, 2918, 2841, overtones Ar = 2100-1700, 1673, 1601, 1457, 1420. ^{1}H NMR (500 MHz, $CDCl_3$) δ: 7.96 (d, *J* = 8.7 Hz, 2H, Ar), 7.28 (m, 2H, Ar), 7.20 (t, *J* = 6.7 Hz, 1H, Ar), 7.13 (d, *J* = 7.5 Hz, 2H, Ar), 6.93 (d, *J* = 8.7 Hz, 2H, Ar), 3.87 (s, 3H, OC*H*$_3$), 3.41 (m, 2H, COC*H*$_2$CH$_2$), 3.17 (m, 2H, Pip-2, Pip-6), 3.07 (m, 2H, CH$_2$C*H*$_2$N), 2.57 (brd, 2H, C*H*$_2$Pip-4), 2.28 (m, 2H, Pip-2, Pip-6), 1.73 (brd, 2H, Pip-3, Pip-5), 1.64 (m, 3H, Pip-3, Pip-4, Pip-5). ^{13}C NMR (125 MHz, $CDCl_3$) δ: 177.5, 163.8, 139.9, 130.5, 129.2, 129.0, 128.3, 126.1, 113.8, 53.7, 52.8, 42.5, 37.1, 34.6, 30.5. UHPLC-ESI-MS: ABS t_R = 1.35, 98% pure (λ = 254 nm), m/z = 338.4 $[M + H]^+$.

The DSC curve showed the typical thermal profile of an anhydrous form with a melting endothermic effect recorded at 191.5 ± 0.1 °C (ΔH_{fus} = 129 ± 7 Jg^{-1}).

3-(4-benzylpiperidin-1-yl)-1-(naphthalen-2-yl)propan-1-one (**15**) By following the General Procedure, starting from 2-bromonaphthalene (311 mg, 1.5 mmol, 1.5 equiv.), 3-(4-benzylpiperidin-1-yl)-*N*-methoxy-*N*-methylpropanamide (290 mg, 1.00 mmol, 1.0 equiv.), *t*-BuLi (1.9 M, 1.32 mL, 2.5 mmol, 2.5 equiv.) and THF (5 mL), the desired product was obtained in 22% (79 mg) as a bright yellow oil after chromatography on silica gel (90:10 etylacetate:methanol) and converted into the corresponding hydrochloride. FT-IR (cm^{-1}): 3059, 3029, 2943, 2921, 2864, overtones Ar = 2000-1700, 1674, 1595, 1495, 1456. ^{1}H NMR (500 MHz, $CDCl_3$) δ: 8.41 (s, 1H, Nap), 7.95 (d, *J* = 8.7 Hz, 1H, Nap), 7.89 (d, *J* = 8.1 Hz, 1H, Nap), 7.80 (t, *J* = 8.9 Hz, 2H, Nap), 7.54-7.46 (m, 2H, Nap), 7.20 (t, *J* = 7.5 Hz, 2H, Ar), 7.11 (t, *J* = 7.3 Hz, 1H, Ar), 7.06 (d, *J* = 7.5 Hz, 2H, Ar), 3.31 (t, *J* = 7.5 Hz, 2H, $COCH_2CH_2$), 2.95 (brd, 2H, Pip-2, Pip-6), 2.85 (t, *J* = 7.6 Hz, 2H, CH_2CH_2N), 2.47 (d, *J* = 7.2 Hz, 2H, CH_2Pip-4), 2.00 (m, 2H, Pip-2, Pip-6), 1.61 (brd, 2H, Pip-3, Pip-5), 1.50 (m, 1H, Pip-4), 1.33 (m, 2H, Pip-3, Pip-5). ^{13}C NMR (125 MHz, $CDCl_3$) δ: 198.9, 140.4, 135.5, 133.9, 132.4, 129.8, 129.5, 129.0, 128.5, 128.4, 128.2, 127.7, 125.8, 123.7, 53.9, 53.4, 43.0, 37.6, 36.1, 31.7. UHPLC-ESI-MS: ABP t_R = 1.62, 98% pure (λ = 254 nm), m/z = 358. $[M + H]^+$.

The thermal profile was typical of an anhydrous form showing the melting endothermic effect at 199.2 ± 0.2 °C (ΔH_{fus} = 178 ± 1 Jg^{-1}).

1-([1,1'-biphenyl]-4-yl)-3-(4-benzylpiperidin-1-yl)propan-1-one (**16**) By following the General Procedure, starting from 4-bromo-1,1'-biphenyl (350 mg, 1.5 mmol, 1.5 equiv.), 3-(4-benzylpiperidin-1-yl)-*N*-methoxy-*N*-methylpropanamide (290 mg, 1.00 mmol, 1.0 equiv.), *t*-BuLi (1.9 M, 1.32 mL, 2.5 mmol, 2.5 equiv.) and THF (5 mL), the desired product was obtained in 23% (84 mg) as a bright yellow oil after chromatography on silica gel (90:10 etylacetate:methanol) and converted into the corresponding hydrochloride. FT-IR (cm^{-1}): 3059, 3029, 2916, overtones Ar = 2100-1700, 1677, 1601, 1457, 1402. ^{1}H NMR (400 MHz, $CDCl_3$) δ: 12.24 (brs, 1H, NH^+), 8.09 (brd, 2H, Ar), 7.70 (brd, 2H, Ar), 7.63 (brd, 2H, Ar), 7.48 (brt, 2H, Ar), 7.43 (brt, 1H, Ar), 7.29-7.13 (m,

5H, Ar), 3.87 (brs, 2H, COC*H*$_2$CH$_2$), 3.58 (brs, 2H, Pip-2, Pip-6), 3.48 (brs, 2H, CH$_2$C*H*$_2$N), 2.71-2.64 (m, 4H, Pip-2, Pip-6, C*H*$_2$Pip-4), 2.08 (brt, 2H, Pip-3, Pip-5), 1.87-1.79 (m, 3H, Pip-3, Pip-4, Pip-5). ^{13}C NMR (100 MHz, $CDCl_3$) δ: 195.7, 146.6, 139.4, 138.9, 134.0, 128.9, 128.4, 128.3, 127.3, 127.2, 126.3, 53.6, 52.1, 41.8, 36.4, 33.3, 28.9. UHPLC-ESI-MS: ABP t_R = 2.37, 95% pure (λ = 254 nm), m/z = 384.4 $[M + H]^+$.

The thermal profile was typical of an anhydrous form showing the melting endothermic effect at 198.9 ± 0.6 °C (ΔH_{fus} = 115 ± 2 Jg^{-1}).

1-phenyl-3-(piperidin-1-yl)propan-1-one (**17**) By following the General Procedure, starting from bromobenzene (236 mg, 1.5 mmol, 1.5 equiv.), *N*-methoxy-*N*-methyl-3-(piperidin-1-yl)propanamide (200 mg, 1.00 mmol, 1.0 equiv.), *t*-BuLi (1.9 M, 1.32 mL, 2.5 mmol, 2.5 equiv.) and THF (5 mL), the desired product was obtained in 29% (63 mg) as a bright yellow oil after chromatography on silica gel (60:40 etylacetate:methanol) and converted into the corresponding hydrochloride. FT-IR (cm^{-1}): 3055, 3021, 2938, 2863, overtones Ar = 2100-1700, 1682, 1597, 1581, 1477, 1456. ^{1}H NMR (500 MHz, $CDCl_3$) δ: 7.95 (dd, *J* = 1.2 and 7.9 Hz, 2H, Ar), 7.55 (m, 1H, Ar), 7.45 (t, *J* = 7.9 Hz, 2H, Ar), 3.24 (t, *J* = 7.4 Hz, 2H, COC*H*$_2$CH$_2$), 2.83 (t, *J* = 7.8 Hz, 2H, CH$_2$C*H*$_2$N), 2.49 (brs, 4H, Pip-2, Pip-6), 1.62 (m, 4H, Pip-3, Pip-5), 1.44 (m, 2H, Pip-4). ^{13}C NMR (125 MHz, $CDCl_3$) δ: 197.1, 136.7, 133.1, 128.6, 128.0, 54.5, 53.7, 36.0, 25.7, 24.0. UHPLC-ESI-MS: ABP t_R = 1.07, 96% pure (λ = 254 nm), m/z = 218.3 $[M + H]^+$.

The thermal profile was typical of an anhydrous form showing the melting endothermic effect at 185.4 ± 0.1 °C (ΔH_{fus} = 147 ± 1 Jg^{-1}).

1-(4-methoxyphenyl)-3-(piperidin-1-yl)propan-1-one (**18**) By following the General Procedure, starting from 1-bromo-4-methoxybenzene (281 mg, 1.5 mmol, 1.5 equiv.), *N*-methoxy-*N*-methyl-3-

(piperidin-1-yl)propanamide (200 mg, 1.00 mmol, 1.0 equiv.), *t*-BuLi (1.9 M, 1.32 mL, 2.5 mmol, 2.5 equiv.) and THF (5 mL), the desired product was obtained in 27% (67 mg) as a bright yellow oil after chromatography on silica gel (60:40 etylacetate:methanol) and converted into the corresponding hydrochloride. FT-IR (cm^{-1}): 2951, 2937, 2875, overtones Ar = 2100-1700, 1672, 1598, 1464, 1442, 1425. ^{1}H NMR (500 MHz, $CDCl_3$) δ: 7.93 (d, *J* = 8.9 Hz, 2H, Ar), 6.91 (d, *J* = 8.7 Hz, 2H, Ar), 3.85 (s, 3H, OC*H*$_3$), 3.17 (t, *J* = 7.4 Hz, 2H, COC*H*$_2$CH$_2$), 2.80 (t, *J* = 7.9 Hz, 2H, CH$_2$C*H*$_2$N), 2.47 (brs, 4H, Pip-2, Pip-6), 1.60 (m, 4H, Pip-3, Pip-5), 1.44 (m, 2H, Pip-4). ^{13}C NMR (125 MHz, $CDCl_3$) δ: 197.8, 163.4, 130.3, 129.9, 113.7, 55.4, 54.5, 53.9, 35.8, 25.8, 24.1. UHPLC-ESI-MS: ABP t_R = 1.24, 98% pure (λ = 254 nm), m/z = 248.3 $[M + H]^+$.

The thermal profile was typical of an anhydrous form showing the melting endothermic effect at 207.3 ± 0.6 °C (ΔH_{fus} = 107 ± 6 Jg^{-1}).

1-(naphthalen-2-yl)-3-(piperidin-1-yl)propan-1-one (**19**) By following the General Procedure, starting from 2-bromonaphthalene (311 mg, 1.5 mmol, 1.5 equiv.), *N*-methoxy-*N*-methyl-3-(piperidin-1-yl)propanamide (200 mg, 1.00 mmol, 1.0 equiv.), *t*-BuLi (1.9 M, 1.32 mL, 2.5 mmol, 2.5 equiv.) and THF (5 mL), the desired product was obtained in 23% (61 mg) as a bright yellow oil after chromatography on silica gel (60:40 etylacetate:methanol) and converted into the corresponding hydrochloride. FT-IR (cm^{-1}): 3037, 2934, 2891, 2855, overtones Ar = 2100-1700, 1676, 1598, 1463. ^{1}H NMR (500 MHz, $CDCl_3$) δ: 8.50 (s, 1H, Nap), 8.02 (d, *J* = 8.5 Hz, 1H, Nap), 7.96 (d, *J* = 8.1 Hz, 1H, Nap), 7.88 (t, *J* = 9.2 Hz, 2H, Nap), 7.62-7.54 (m, 2H, Nap), 3.43 (t, *J* = 7.3 Hz, 2H, COC*H*$_2$CH$_2$), 2.95 (t, *J* = 7.2 Hz, 2H, CH$_2$C*H*$_2$N), 2.59 (brs, 4H, Pip-2, Pip-6), 1.68 (m, 4H, Pip-3, Pip-5), 1.49 (m, 2H, Pip-4). ^{13}C NMR (125 MHz, $CDCl_3$) δ: 198.9, 135.6, 134.0, 132.5, 129.9, 129.6, 128.5, 127.7, 126.8, 123.7, 54.5, 53.7, 36.0, 25.5, 23.9. UHPLC-ESI-MS: ABS t_R = 1.09, 95% pure (λ = 254 nm), m/z = 268.3 $[M + H]^+$.

The thermal profile was typical of an anhydrous form showing the melting endothermic effect at 188.7 ± 0.2 °C (ΔH_{fus} = 130 ± 3 Jg^{-1}).

1-([1,1'-biphenyl]-4-yl)-3-(piperidin-1-yl)propan-1-one (**20**) By following the General Procedure, starting from 4-bromo-1,1'-biphenyl (350 mg, 1.5 mmol, 1.5 equiv.), *N*-methoxy-*N*-methyl-3-(piperidin-1-yl)propanamide (200 mg, 1.00 mmol, 1.0 equiv.), *t*-BuLi (1.9 M, 1.32 mL, 2.5 mmol, 2.5 equiv.) and THF (5 mL), the desired product was obtained in 35% (103 mg) as a bright yellow oil after chromatography on silica gel (60:40 etylacetate:methanol) and converted into the corresponding hydrochloride. FT-IR (cm^{-1}): 3055, 3027, 2934, overtones Ar = 2100-1700, 1680, 1605, 1560, 1449, 1430. ^{1}H NMR (500 MHz, $CDCl_3$) δ: 8.04 (d, *J* = 8.3 Hz, 2H, Ar), 7.68 (d, *J* = 8.4 Hz, 2H, Ar), 7.62 (d, *J* = 8.0 Hz, 2H, Ar), 7.47 (t, *J* = 7.3 Hz, 2H, Ar), 7.41 (t, *J* = 7.2 Hz, 1H, Ar), 3.27 (t, *J* = 7.4 Hz, 2H, COC*H*$_2$CH$_2$), 2.86 (t, *J* = 7.8 Hz, 2H, CH$_2$C*H*$_2$N), 2.51 (brs, 4H, Pip-2, Pip-6), 1.63 (m, 4H, Pip-3, Pip-5), 1.47 (m, 2H, Pip-4). ^{13}C NMR (125 MHz, $CDCl_3$) δ: 198.8, 145.7, 139.8, 135.5, 128.9, 128.6, 128.2, 127.2, 54.6, 53.8, 36.2, 25.7, 24.1. UHPLC-ESI-MS: ABP t_R = 1.89, 95% pure (λ = 254 nm), m/z = 294.3 $[M + H]^+$.

The thermal profile was typical of an anhydrous form showing the melting endothermic effect at 190.6 ± 0.9 °C (ΔH_{fus} = 61 ± 4 Jg^{-1}).

3-morpholino-1-phenylpropan-1-one (**21**) By following the General Procedure, starting from bromobenzene (236 mg, 1.5 mmol, 1.5 equiv.), *N*-methoxy-*N*-methyl-3-morpholinopropanamide (202 mg, 1.00 mmol, 1.0 equiv.), *t*-BuLi (1.9 M, 1.32 mL, 2.5 mmol, 2.5 equiv.) and THF (5 mL), the desired product was obtained in 30% (66 mg) as a bright yellow oil after chromatography on silica gel (90:10 etylacetate:methanol) and converted into the corresponding hydrochloride. FT-IR (cm^{-1}): 3086, 2981, 2930, 2872, overtones Ar = 2100-1700, 1685, 1597, 1584, 1445, 1405. ^{1}H NMR (500

MHz, $CDCl_3$) δ: 7.94 (dd, *J* = 1.3 and 7.2 Hz, 2H, Ar), 7.55 (m, 1H, Ar), 7.46 (t, *J* = 7.8 Hz, 2H, Ar), 3.70 (t, *J* = 4.6 Hz, 4H, Mor-3, Mor-5), 3.18 (t, *J* = 7.3 Hz, 2H, $COCH_2CH_2$), 2.83 (t, *J* = 7.7 Hz, 2H, CH_2CH_2N), 2.50 (brs, 4H, Mor-2, Mor-6). ^{13}C NMR (125 MHz, $CDCl_3$) δ: 198.9, 136.7, 133.1, 128.6, 128.0, 66.8, 53.6, 53,4, 35.9. UHPLC-ESI-MS: ABP t_R = 0.82, 99% pure (λ = 254 nm), m/z = 220.2 $[M + H]^+$.

The thermal profile was typical of an anhydrous form showing the melting endothermic effect at 178.1 ± 0.8 °C (ΔH_{fus} = 160 ± 2 Jg^{-1}).

1-(4-methoxyphenyl)-3-morpholinopropan-1-one (**22**) By following the General Procedure, starting from 1-bromo-4-methoxybenzene (281 mg, 1.5 mmol, 1.5 equiv.), *N*-methoxy-*N*-methyl-3-morpholinopropanamide (202 mg, 1.00 mmol, 1.0 equiv.), *t*-BuLi (1.9 M, 1.32 mL, 2.5 mmol, 2.5 equiv.) and THF (5 mL), the desired product was obtained in 38% (95 mg) as a bright yellow oil after chromatography on silica gel (90:10 etylacetate:methanol) and converted into the corresponding hydrochloride. FT-IR (cm^{-1}): 2990, 2954, 2932, 2857, overtones Ar = 2100-1700, 1674, 1597, 1427. ^1H NMR (500 MHz, $CDCl_3$) δ: 7.94 (d, *J* = 8.9 Hz, 2H, Ar), 6.93 (d, *J* = 8.9 Hz, 2H, Ar), 3.87 (s, 3H, OCH_3), 3.74 (m, 4H, Mor-3, Mor-5), 3.17 (t, *J* = 7.3 Hz, 2H, $COCH_2CH_2$), 2.86 (t, *J* = 7.2 Hz, 2H, CH_2CH_2N), 2.47 (brs, 4H, Mor-2, Mor-6),. ^{13}C NMR (125 MHz, $CDCl_3$) δ: 197.3, 163.5, 130.3, 129.8, 66.7, 55.5, 53.6, 35.4. UHPLC-ESI-MS: ABP t_R = 0.84, > 99% pure (λ = 254 nm), m/z = 250.2 $[M + H]^+$.

The thermal profile was typical of an anhydrous form showing the melting endothermic effect at 211.0 ± 0.9 °C (ΔH_{fus} = 244 ± 5 Jg^{-1}).

3-morpholino-1-(naphthalen-2-yl)propan-1-one (**23**) By following the General Procedure, starting from 2-bromonaphthalene (311 mg, 1.5 mmol, 1.5 equiv.), *N*-methoxy-*N*-methyl-3-

morpholinopropanamide (202 mg, 1.00 mmol, 1.0 equiv.), *t*-BuLi (1.9 M, 1.32 mL, 2.5 mmol, 2.5 equiv.) and THF (5 mL), the desired product was obtained in 41% (110 mg) as a bright yellow oil after chromatography on silica gel (90:10 etylacetate:methanol) and converted into the corresponding hydrochloride. FT-IR (cm^{-1}): 3018, 2924, 2863, overtones Ar = 2100-1700, 1687, 1594, 1469, 1436. ^{1}H NMR (500 MHz, $CDCl_3$) δ: 8.48 (s, 1H, Nap), 8.02 (dd, *J* = 1.5 and 8.5 Hz, 1H, Nap), 7.95 (d, *J* = 8.5 Hz, 1H, Nap), 7.88 (t, *J* = 9.5 Hz, 2H, Nap), 7.61-7.53 (m, 2H, Nap), 3.76 (t, *J* = 4.5 Hz, 4H, Mor-3, Mor-5), 3.37 (t, *J* = 7.0 Hz, 2H, $COCH_2CH_2$), 2.94 (t, *J* = 7.5 Hz, 2H, CH_2CH_2N), 2.60 (brs, 4H, Mor-2, Mor-6). ^{13}C NMR (125 MHz, $CDCl_3$) δ: 198.6, 135.6, 134.0, 132.4, 129.8, 129.5, 128.5, 127.7, 126.8, 123.7, 66.6, 53.6, 53.5, 35.7. UHPLC-ESI-MS: ABP t_R = 1.48, 99% pure (λ = 254 nm), m/z = 270.3 $[M + H]^+$.

The thermal profile was typical of an anhydrous form showing the melting endothermic effect at 198.9 ± 0.4 °C (ΔH_{fus} = 153 ± 5 Jg^{-1}).

1-([1,1'-biphenyl]-4-yl)-3-morpholinopropan-1-one (**24**) By following the General Procedure, starting from 4-bromo-1,1'-biphenyl (350 mg, 1.5 mmol, 1.5 equiv.), *N*-methoxy-*N*-methyl-3-morpholinopropanamide (202 mg, 1.00 mmol, 1.0 equiv.), *t*-BuLi (1.9 M, 1.32 mL, 2.5 mmol, 2.5 equiv.) and THF (5 mL), the desired product was obtained in 37% (109 mg) as a bright yellow oil after chromatography on silica gel (90:10 etylacetate:methanol) and converted into the corresponding hydrochloride. FT-IR (cm^{-1}): 3023, 2861, overtones Ar = 2100-1700, 1683, 1603, 1451. ^{1}H NMR (500 MHz, $CDCl_3$) δ: 8.03 (d, *J* = 8.4 Hz, 2H, Ar), 7.68 (d, *J* = 8.4 Hz, 2H, Ar), 7.62 (d, *J* = 7.6 Hz, 2H, Ar), 7.47 (t, *J* = 7.4 Hz, 2H, Ar), 7.40 (t, *J* = 7.4 Hz, 1H, Ar), 3.73 (t, *J* = 4.6 Hz, 4H, Mor-3, Mor-5), 3.23 (t, *J* = 7.4 Hz, 2H, $COCH_2CH_2$), 2.87 (t, *J* = 7.7 Hz, 2H, CH_2CH_2N), 2.54 (brs, 4H, Mor-2, Mor-6). ^{13}C NMR (125 MHz, $CDCl_3$) δ: 198.4, 145.8, 139.7, 135.4, 128.9, 128.6, 128.2,

127.2, 66.8, 53.6, 53.5, 35.9. UHPLC-ESI-MS: ABP t_R = 1.74, 99% pure (λ = 254 nm), m/z = 296.3 $[M + H]^+$.

The thermal profile showed a double endothermic effect with a peak at 207.5 ± 0.1 °C and a shoulder at 196.8 ± 0.5 °C, with a total area corresponding to an enthalpy value of 165 ± 1 Jg^{-1}. This behavior could be attributed to the presence of two solid phases that should be better investigated.

4-benzyl-1-(4-oxo-4-phenylbutyl)piperidin-1-ium hydrochloride (**25**) By following the General Procedure, starting from bromobenzene (236 mg, 1.5 mmol, 1.5 equiv.), 4-(4-benzylpiperidin-1-yl)-*N*-methoxy-*N*-methylbutanamide (304 mg, 1.00 mmol, 1.0 equiv.), *t*-BuLi (1.9 M, 1.32 mL, 2.5 mmol, 2.5 equiv.) and THF (5 mL), the desired product was obtained in 31% (100 mg) as a bright yellow oil after chromatography on silica gel (80:20 etylacetate:methanol) and converted into the corresponding hydrochloride. FT-IR (cm^{-1}): 3025, 2930, 2849, overtones Ar = 2100-1700, 1680, 1595, 1580, 1452, 1414. ^{1}H NMR (500 MHz, $CDCl_3$) δ: 12.06 (brs, 1H, N*H*$^+$), 7.94 (d, *J* = 7.2 Hz, 2H, Ar), 7.59 (t, *J* = 7.4 Hz, 1H, Ar), 7.47 (t, *J* = 7.3 Hz, 2H, Ar), 7.29 (t, *J* = 7.1 Hz, 2H, Ar), 7.22 (t, *J* = 7.1 Hz, 2H, Ar), 7.13 (d, *J* = 7.0 Hz, 1H, Ar), 3.60 (brd, 2H, Pip-2, Pip-6), 3.22 (brs, 2H, $COCH_2CH_2$), 3.04 (brs, 2H, CH_2CH_2N), 2.63 (m, 4H, CH_2Pip-4, Pip-2, Pip-6), 2.34 (brs, 2H, $CH_2CH_2CH_2$), 2.10 (m, 2H, Pip-3, Pip-5), 1.83 (d, 2H, Pip-3, Pip-5), 1.60 (m, 1H, Pip-4). ^{13}C NMR (125 MHz, $CDCl_3$) δ: 198.4, 139.1, 136.1, 133.7, 129.0, 128.8, 128.5, 128.0, 126.4, 57.0, 53.1, 41.9, 36.7, 35.6, 28.9, 18.0. UHPLC-ESI-MS: ABP t_R = 2.00, > 99% pure (λ = 254 nm), m/z = 322.5 $[M + H]^+$.

The thermal profile showed two well defined endothermic effects; the first at 142.8 ± 0.3 °C attributable to a lower melting phase (ΔH_{fus} = 60 ± 1 Jg^{-1}), followed at 148.0 ±0.3 °C by the exothermic recrystallization into the higher melting phase (T_{fus} = 157.6 ± 0.3 °C, ΔH_{fus} = 30 ± 3 Jg^{-1}).

4-benzyl-1-(4-(4-methoxyphenyl)-4-oxobutyl)piperidin-1-ium hydrochloride (**26**) By following the General Procedure, starting from 1-bromo-4-methoxybenzene (281 mg, 1.5 mmol, 1.5 equiv.), 4-(4-benzylpiperidin-1-yl)-*N*-methoxy-*N*-methylbutanamide (304 mg, 1.00 mmol, 1.0 equiv.), *t*-BuLi (1.9 M, 1.32 mL, 2.5 mmol, 2.5 equiv.) and THF (5 mL), the desired product was obtained in 30% (106 mg) as a bright yellow oil after chromatography on silica gel (80:20 etylacetate:methanol) and converted into the corresponding hydrochloride. FT-IR (cm^{-1}): 3024, 3003, 2922, overtones Ar = 2100-1700, 1677, 1603, 1451. ^{1}H NMR (500 MHz, $CDCl_3$) δ: 12.03 (brs, 1H, N*H*$^+$), 7.92 (d, *J* = 8.1 Hz, 2H, Ar), 7.29 (t, *J* = 7.2 Hz, 2H, Ar), 7.21 (t, *J* = 7.2 Hz, 1H, Ar), 7.12 (d, *J* = 7.1 Hz, 2H, Ar), 6.92 (d, *J* = 8.0 Hz, 2H, Ar), 3.87 (s, 3H, OC*H*$_3$), 3.59 (brd, 2H, Pip-2, Pip-6), 3.16 (brs, 2H, COC*H*$_2$CH$_2$), 3.03 (brs, 2H, CH$_2$C*H*$_2$N), 2.62 (m, 4H, C*H*$_2$Pip-4, Pip-2, Pip-6), 2.32 (brs, 2H, CH$_2$C*H*$_2$CH$_2$), 2.08 (m, 2H, Pip-3, Pip-5), 1.82 (d, 2H, Pip-3, Pip-5), 1.73 (brs, 1H, Pip-4). ^{13}C NMR (125 MHz, $CDCl_3$) δ: 196.9, 163.8, 139.1, 130.3, 129.2, 129.0, 128.5, 126.3, 113.9, 57.0, 55.5, 53.0, 41.9, 36.6, 35.1, 28.8, 18.1. UHPLC-ESI-MS: ABS t_R = 1.43, 99% pure (λ = 254 nm), m/z = 352.4 $[M + H]^+$.

The thermal profile showed two endothermic effects; the first of little intensity at 119.8 ± 0.9 °C, not associated with a mass loss in TGA curve, was probably due to a metastable phase melting, and the second instead related to a stable phase melting at 157.4 ± 0.5 °C (ΔH_{fus} = 61 ± 1 Jg^{-1}).

4-benzyl-1-(4-(3-methoxyphenyl)-4-oxobutyl)piperidin-1-ium hydrochloride (**27**) By following the General Procedure, starting from 1-bromo-3-methoxybenzene (281 mg, 1.5 mmol, 1.5 equiv.), 4-(4-benzylpiperidin-1-yl)-*N*-methoxy-*N*-methylbutanamide (304 mg, 1.00 mmol, 1.0 equiv.), *t*-BuLi (1.9 M, 1.32 mL, 2.5 mmol, 2.5 equiv.) and THF (5 mL), the desired product was obtained in 33% (116 mg) as a bright yellow oil after chromatography on silica gel (80:20 etylacetate:methanol) and

converted into the corresponding hydrochloride. FT-IR (cm^{-1}): 3022, 2946, 2861, overtones Ar = 2100-1700, 1687, 1595, 1486, 1465. ^{1}H NMR (500 MHz, $CDCl_3$) δ: 12.04 (brs, 1H, N*H*$^{+}$), 7.52 (d, *J* = 7.4 Hz, 1H, Ar), 7.45 (s, 1H, Ar), 7.37 (t, *J* = 7.9 Hz, 1H, Ar), 7.29 (t, *J* = 7.2 Hz, 2H, Ar), 7.21 (t, *J* = .7.2 Hz, 1H, Ar), 7.13 (m, 3H, Ar), 3.85 (s, 3H, OC*H*$_3$), 3.59 (brd, 2H, Pip-2, Pip-6), 3.21 (brs, 2H, COC*H*$_2$CH$_2$), 3.03 (brs, 2H, CH$_2$C*H*$_2$N), 2.63 (m, 4H, C*H*$_2$Pip-4, Pip-2, Pip-6), 2.33 (brs, 2H, CH$_2$C*H*$_2$CH$_2$), 2.09 (m, 2H, Pip-3, Pip-5), 1.83 (d, 2H, Pip-3, Pip-5), 1.73 (brs, 1H, Pip-4). ^{13}C NMR (125 MHz, $CDCl_3$) δ: 198.3, 159.8, 139.1, 137.4, 129.8, 129.0, 128.5, 126.4, 120.6, 120.1, 112.0, 56.9, 55.5, 53.0, 41.9, 36.6, 35.6, 28.8, 18.0. UHPLC-ESI-MS: ABP t_R = 2.08, 99% pure (λ = 254 nm), m/z = 352.5 $[M + H]^+$.

The thermal profile showed an endothermic effect at 148.9 ± 0.1 °C with a shoulder at 153.9 ± 0.2 (ΔH_{fus} = 76 ± 3 Jg^{-1}).

4-benzyl-1-(4-(naphthalen-2-yl)-4-oxobutyl)piperidin-1-ium hydrochloride (**28**) By following the General Procedure, starting from 2-bromonaphthalene (311 mg, 1.5 mmol, 1.5 equiv.), 4-(4-benzylpiperidin-1-yl)-*N*-methoxy-*N*-methylbutanamide (304 mg, 1.00 mmol, 1.0 equiv.), *t*-BuLi (1.9 M, 1.32 mL, 2.5 mmol, 2.5 equiv.) and THF (5 mL), the desired product was obtained in 41% (152 mg) as a bright yellow oil after chromatography on silica gel (80:20 etylacetate:methanol) and converted into the corresponding hydrochloride. FT-IR (cm^{-1}): 3055, 3027, 2937, 2907, overtones Ar = 2100-1700, 1681, 1496, 1441. ^{1}H NMR (500 MHz, $CDCl_3$) δ: 12.06 (brs, 1H, N*H*$^{+}$), 8.50 (s, 1H, Nap), 7.98 (d, *J* = 8.1 Hz, 2H, Nap), 7.88 (t, *J* = 10.0 Hz, 2H, Nap), 7.61 (t, *J* = 6.8 Hz, 1H, Nap), 7.57 (t, *J* = 6.9 Hz, 1H, Nap), 7.29 (t, *J* = 7.1 Hz, 2H, Ar), 7.22 (t, *J* = 7.1 Hz, 1H, Ar), 7.14 (d, *J* = 7.1 Hz, 2H, Ar), 3.62 (brd, 2H, Pip-2, Pip-6), 3.37 (brs, 2H, COC*H*$_2$CH$_2$), 3.09 (brs, 2H, CH$_2$C*H*$_2$N), 2.64 (m, 4H, C*H*$_2$Pip-4, Pip-2, Pip-6), 2.41 (brs, 2H, CH$_2$C*H*$_2$CH$_2$), 2.11 (m, 2H, Pip-3, Pip-5), 1.84 (d, 2H, Pip-3, Pip-5), 1.71 (m, 1H, Pip-4). ^{13}C NMR (125 MHz, $CDCl_3$) δ: 198.4, 139.1, 135.6, 133.4,

132.4, 130.1, 129.7, 129.0, 128.8, 128.7, 128.5, 127.8, 126.4, 123.4, 57.0, 53.1, 41.9, 36.6, 35.7, 28.9, 18.2. UHPLC-ESI-MS: ABS t_R = 1.67, > 99% pure (λ = 254 nm), m/z = 372.5 $[M + H]^+$.

The thermal profile showed a first endothermic effect at 78.1 ± 0.6 °C (ΔH = 103 ± 4 Jg^{-1}) attributable to the desolvation of the sample. The TGA mass loss of 10.0 ± 0.1%, recorded in the same DSC temperature range, was in agreement with the theoretical loss of one molecule of ethanol for molecule of compound (10.15%), allowing to presume the crystallization of a solvatomorph. The second endothermic effect at 162.9 ± 0.4°C (ΔH_{fus} = 58 ± 3 Jg^{-1}) was due to the melting of the anhydrous form.

4-benzyl-1-(4-(6-methoxynaphthalen-2-yl)-4-oxobutyl)piperidin-1-ium hydrochloride (**29**) By following the General Procedure, starting from 2-bromo-6-methoxynaphthalene (256 mg, 1.5 mmol, 1.5 equiv.), 4-(4-benzylpiperidin-1-yl)-*N*-methoxy-*N*-methylbutanamide (304 mg, 1.00 mmol, 1.0 equiv.), *t*-BuLi (1.9 M, 1.32 mL, 2.5 mmol, 2.5 equiv.) and THF (5 mL), the desired product was obtained in 25% (101 mg) as a bright yellow oil after chromatography on silica gel (80:20 etylacetate:methanol) and converted into the corresponding hydrochloride. FT-IR (cm^{-1}): 3024, 2936, overtones Ar = 2100-1700, 1674, 1482, 1409. ^{1}H NMR (500 MHz, $CDCl_3$) δ: 12.06 (brs, 1H, N*H*$^+$), 8.41 (s, 1H, Nap), 7.95 (d, *J* = 8.3 Hz, 1H, Nap), 7.85 (t, *J* = 8.7 Hz, 1H, Nap), 7.76 (d, *J* = 8.4 Hz, 1H, Nap), 7.29 (t, *J* = 7.1 Hz, 2H, Ar), 7.21 (t, 2H, Ar, Nap), 7.13 (d, 3H, Ar, Nap), 3.94 (s, 3H, CH_3), 3.61 (brd, 2H, Pip-2, Pip-6), 3.32 (brs, 2H, COC*H*$_2$$CH_2$), 3.08 (brs, 2H, CH_2C*H*$_2$N), 2.63 (m, 4H, C*H*$_2$Pip-4, Pip-2, Pip-6), 2.38 (brs, 2H, CH_2C*H*$_2$$CH_2$), 2.09 (m, 2H, Pip-3, Pip-5), 1.83 (d, 2H, Pip-3, Pip-5), 1.74 (m, 1H, Pip-4). ^{13}C NMR (125 MHz, $CDCl_3$) δ: 198.1, 159.9, 139.1, 137.5, 131.5, 131.3, 129.9, 129.0, 128.5, 127.7, 127.3, 126.4, 124.2, 119.9, 105.6, 57.0, 55.4, 53.0, 41.9, 36.6, 35.4, 28.9, 18.2,. UHPLC-ESI-MS: ABS t_R = 1.71, > 99% pure (λ = 254 nm), m/z = 4022.5 $[M + H]^+$.

The thermal profile showed, at 170.5 ± 0.6 °C, an endothermic effect due to a lower melting phase (ΔH_{fus} = 53 ± 4 Jg^{-1}), followed at 178.1 ± 0.5 °C by the exothermic recrystallization into the higher melting phase (T_{fus} = 206.7 ± 0.2 °C, ΔH_{fus} = 68 ± 5 Jg^{-1}).

1-(4-([1,1'-biphenyl]-4-yl)-4-oxobutyl)-4-benzylpiperidin-1-ium hydrochloride (**30**) By following the General Procedure, starting from 4-bromo-1,1'-biphenyl (350 mg, 1.5 mmol, 1.5 equiv.), 4-(4-benzylpiperidin-1-yl)-*N*-methoxy-*N*-methylbutanamide (304 mg, 1.00 mmol, 1.0 equiv.), *t*-BuLi (1.9 M, 1.32 mL, 2.5 mmol, 2.5 equiv.) and THF (5 mL), the desired product was obtained in 26% (103 mg) as a bright yellow oil after chromatography on silica gel (80:20 etylacetate:methanol) and converted into the corresponding hydrochloride. FT-IR (cm^{-1}): 3083, 3025, 2995, 2850, overtones Ar = 2100-1700, 1684, 1604. ^{1}H NMR (500 MHz, $CDCl_3$) δ: 12.07 (brs, 1H, N*H*$^{+}$), 8.02 (d, *J* = 6.3 Hz, 2H, Ar), 7.69 (d, *J* = 6.3 Hz, 2H, Ar), 7.62 (d, *J* = 7.2 Hz, 2H, Ar), 7.46 (t, *J* = 7.1 Hz, 2H, Ar), 7.41 (t, *J* = 7.2 Hz, 1H, Ar), 7.30 (t, *J* = 7.1 Hz, 2H, Ar), 7.22 (t, *J* = 7.2 Hz, 1H, Ar), 7.14 (d, *J* = 7.0 Hz, 2H, Ar), 3.61 (brd, 2H, Pip-2, Pip-6), 3.26 (brs, 2H, COC*H*$_2$CH$_2$), 3.07 (brs, 2H, CH$_2$C*H*$_2$N), 2.64 (m, 4H, C*H*$_2$Pip-4, Pip-2, Pip-6), 2.37 (brs, 2H, CH$_2$C*H*$_2$CH$_2$), 2.11 (m, 2H, Pip-3, Pip-5), 1.85 (d, 2H, Pip-3, Pip-5), 1.73 (m, 1H, Pip-4). ^{13}C NMR (125 MHz, $CDCl_3$) δ: 198.0, 146.2, 139.6, 139.1, 134.8, 129.0, 128.7, 128.5, 128.4, 127.4, 127.2, 126.4, 57.0, 53.2, 41.9, 36.7, 35.7, 28.9, 18.1,. UHPLC-ESI-MS: ABS t_R = 1.81, 98% pure (λ = 254 nm), m/z = 398.4 $[M + H]^+$.

The thermal profile showed an exothermic effect at 168.7 ± 0.9 °C, probably attributable to a crystallization of an amorphous fraction of sample, induced by heating. The melting of the anhydrous form was then recorded at 216.4 ± 0.4 °C (ΔH_{fus} = 84 ± 1 Jg^{-1}).

4.5. Physicochemical and pharmacokinetic predictions

The physicochemical properties of compounds **7-30** were calculated by using Chemicalize online property explorer. The *in-silico* ability in crossing the BBB was calculated by using the CNS Multiparameter Optimization Desirability (CNS MPO) tool.

4.6. Binding assays

4.6.1. Materials

Guinea pig brains for the S1R binding assays were commercially available (Harlan–Winkelmann, Borchen, Germany). Homogenizer: Elvehjem Potter (B. Braun Biotech International, Melsungen, Germany) and Soniprep 150, MSE, London, UK). Centrifuges: Cooling centrifuge model Rotina 35R (Hettich, Tuttlingen, Germany) and High-speed cooling centrifuge model Sorvall RC-5C plus (Thermo Fisher Scientific, Langenselbold, Germany). Multiplates: standard 96-well multiplates (Diagonal, Muenster, Germany). Shaker: self-made device with adjustable temperature and tumbling speed (scientific workshop of the institute). Vortexer: Vortex Genie 2 (Thermo Fisher Scientific, Langenselbold, Germany). Harvester: MicroBeta FilterMate-96 Harvester. Filter: Printed Filtermat Type A and B. Scintillator: Meltilex (Type A or B) solid-state scintillator. Scintillation analyzer: MicroBeta Trilux (all PerkinElmer LAS, Rodgau-Jügesheim, Germany). Chemicals and reagents were purchased from various commercial sources and were of analytical grade.

4.6.2. Preparation of membrane homogenates from guinea pig brain cortex

Five guinea pig brains were homogenized with the potter (500–800 rpm, 10 up-and-down strokes) in six volumes of cold 0.32 M sucrose. The suspension was centrifuged at 1200 x g for 10 min at 4 °C. The supernatant was separated and centrifuged at 23500 x g for 20 min at 4 °C. The pellet was resuspended in 5–6 volumes of buffer (50 mM Tris, pH 7.4) and centrifuged again at 23500 g (20

min, 4 °C). This procedure was repeated twice. The final pellet was resuspended in 5–6 volumes of buffer and frozen (-80 °C) in 1.5 mL portions containing ~1.5 (mg protein)mL^{-1}.

4.6.3. Preparation of membrane homogenates from rat liver

Two rat livers were cut into small pieces and homogenized with the potter (500-800 rpm, 10 up-and-down strokes) in six volumes of cold 0.32M sucrose. The suspension was centrifuged at 1200 x g for 10 min at 4 °C. The supernatant was separated and centrifuged at 31,000 x g for 20 min at 4 °C. The pellet was resuspended in 5-6 volumes of buffer (50mM TRIS, pH 8.0) and incubated at rt for 30 min. After the incubation, the suspension was centrifuged again at 31000 x g for 20 min at 4 °C. The final pellet was resuspended in 5-6 vol of buffer and stored at -80 °C in 1.5 mL portions containing about 2mg protein/mL.

4.6.4. Cell culture and preparation of membrane homogenates from GluN2B cells

Mouse L(tk-) cells stably transfected with the dexamethasone inducible eukaryotic expression vectors pMSG GluN1a, pMSG GluN2B (1:5 ratio) were grown in Modified Earl's Medium (MEM) containing 10% of standardized FCS (Biochrom AG, Berlin, Germany).

The expression of the NMDA receptor at the cell surface was induced after the cell density of the adherent growing cells had reached approximately 90% of confluency. For the induction, the original growth medium was replaced by growth medium containing 4 µM dexamethasone and 4 µM ketamine (final concentration). After 24 h, the cells were rinsed with phosphate buffered saline solution (PBS, Biochrom AG, Berlin, Germany), harvested by mechanical detachment and pelleted (10 min, 5000 x g).

For the binding assay, the cell pellet was resuspended in PBS solution and the number of cells was determined using a Scepter® cell counter (MERCK Millipore, Darmstadt, Germany). Subsequently,

the cells were lysed by sonication (4 °C, 6 x 10 s cycles with breaks of 10 s). The resulting cell fragments were centrifuged with a high performance cool centrifuge (23500 x g, 4 °C). The supernatant was discarded and the pellet was resuspended in a defined volume of PBS yielding cell fragments of approximately 500000 cells/mL. The suspension of membrane homogenates was sonicated again (4 °C, 2 x 10 s cycles with a break of 10 s) and stored at -80 °C.

4.6.5. General protocol for binding assays

The test compound solutions were prepared by dissolving ~10 µmol (usually 2–4 mg) of test compound in DMSO so that a 10 mM stock solution was obtained. To obtain the required test solutions for the assay, the DMSO stock solution was diluted with the respective assay buffer. The filtermats were presoaked in 0.5% aqueous polyethylenamine solution for 2 h at rt before use. All binding experiments were carried out in duplicate in 96-well multiplates. The concentrations given are the final concentrations in the assay. Generally, the assays were performed by addition of 50 µL of the respective assay buffer, 50 µL test compound solution at various concentrations (10^{-5}, 10^{-6}, 10^{-7}, 10^{-8}, 10^{-9} and 10^{-10} M), 50 µL of corresponding radioligand solution, and 50 µL of the respective receptor preparation into each well of the multiplate (total volume 200 µL). The receptor preparation was always added last. During the incubation, the multiplates were shaken at a speed of 500–600 rpm at the specified temperature. Unless otherwise noted, the assays were terminated after 120 min by rapid filtration using the harvester. During the filtration each well was washed five times with 300 µL of water. Subsequently, the filtermats were dried at 95 °C. The solid scintillator was melted on the dried filtermats at 95 °C for 5 min. After solidifying of the scintillator at RT, the trapped radioactivity in the filtermats was measured with the scintillation analyzer. Each position on the filtermat corresponding to one well of the multiplate was measured for 5 min with the [^{3}H]-counting protocol. The overall counting efficiency was 20%. The IC_{50} values were calculated with GraphPad

Prism 3.0 (GraphPad Software, San Diego, CA, USA) by nonlinear regression analysis. The IC_{50} values were subsequently transformed into Ki values using the equation of Cheng and Prusoff. The Ki values are given as mean value ±SEM from three independent experiments.

4.6.6. S1R binding assay

The assay was performed with the radioligand [^{3}H](+)-pentazocine (22.0 Ci mmol^{-1}; PerkinElmer). The thawed membrane preparation of guinea pig brain cortex (~100 µg protein) was incubated with various concentrations of test compounds, 2 nM [^{3}H](+)-pentazocine, and Tris buffer (50 mM, pH 7.4) at 37°C. The nonspecific binding was determined with 10 mM unlabeled (+)-pentazocine. The Kd value of (+)-pentazocine is 2.9 nM.

4.6.7. S2R binding assay

The assay was performed using 150 µg of rat liver homogenate were incubated for 120 min at room temperature with 3 nM [^{3}H]-DTG (Perkin–Elmer, specific activity 58.1 Ci mmol^{-1}) in 50 mM Tris–HCl, pH 8.0, 0.5 mL final volume. (+)-pentazocine (100 nM) and haloperidol (10 µM) were used to mask S1R and to define non-specific binding, respectively.

4.6.8. GluN2 binding assay

The competitive binding assay was performed with the radioligand [^{3}H]-ifenprodil (60 Ci/mmol; BIOTREND, Cologne, Germany). The thawed cell membrane preparation from the transfected L(tk-) cells (about 20 µg protein) was incubated with various concentrations of test compounds, 5 nM [^{3}H]-ifenprodil, and TRIS/EDTAbuffer (5mM TRIS/1mM EDTA, pH 7.5) at 37 °C. The non-specific binding was determined with 10 mM unlabeled ifenprodil. The Kd value of ifenprodil is 7.6 nM.

4.7. Inhibition of AChE

AChE inhibitory activity of compounds **7-30** were determined by the modified Ellman's method. Briefly, stock solutions of tested compounds (5.0 mM) were prepared in DMSO and diluted using 0.1 M KH_2PO_4/K_2HPO_4 buffer (pH 8.0) to afford a final concentration range between 1 – 50 μM. Enzyme solutions were prepared by dissolving lyophilized powder in double-distilled water. The assay solution consisted of 845 μL of 0.1 M phosphate buffer KH_2PO_4/K_2HPO_4, 25 μL of AChE solution (0.22 U/mL, E.C. 3.1.1.7, from electric eel) and 10 μL of various concentrations of test compounds, which was allowed to stand for 5 min at 25 °C before 100 μL of 0.01 M DTNB were added. The reaction was started by addition of 20 μL of the 0.075 M substrate solution (acetylthiocholine iodide) and exactly 2 min after substrate addition, the absorption was measured at 25 °C at 412 nm. In enzyme-free assay systems the non-enzymatic hydrolysis of acetylthiocholine iodide was measured, and the results were employed as blank. In control experiments, inhibitor-free assay systems were utilized to measure the full activity. A positive control of Donepezil was used to afford a final concentration range between 10 nM – 50 μM. The percent inhibition was calculated, using the expression: $(1 - A_i/A_c) \times 100$, where A_i and A_c are the absorbances obtained for AChE in the presence and absence of the inhibitors, respectively, after subtracting the respective background. Each experiment was performed in triplicate, and the mean ± standard deviation was calculated. Data from concentration-inhibition experiments of the inhibitors were calculated by nonlinear regression analysis, using the Excel program.

4.8. *In silico* studies

4.8.1. Molecular dynamic simulations

S1R crystal structure in complex with 4-IBP (pdb code 5hk2) [41] was retrieved from the Protein Data Bank [42] and used to investigate the dynamic properties of the receptor. Instead, the X-ray

structure of AChE was available in complex with Donepezil (pdb code 4ey7) [43] and we relied on it for molecular docking of our novel compounds.

Molecular dynamic (MD) simulations of S1R were performed in a membrane environment, in the *holo* form (without any ligand) and in complex with the co-crystallized ligand. Structures were prepared with MOE [44] dedicated tools: hydrogen atoms and missing side chains were added. Atomic charges were calculated and the protonation state determined at physiological conditions (pH 7.4). N- and C-termini were capped with acetyl and N-methyl groups, respectively. Salt, detergent and bulk water molecules were removed from the crystal structures, whilst water molecules which were present in the binding site were maintained. The membrane was built around the three alpha helices by using the CHARMM-GUI membrane builder [45]. The protein was embedded in a heterogeneous membrane, composed of POPC (palmitoyl-oleoyl-phosphatidyl-choline) and cholesterol in 3:1 ratio. Potassium ions were added in order to neutralize the system. MD simulations were performed with the AMBER force field and analyzed with Amber tools [46]. The ligand was parametrized by using Antechamber [47] and Parmchk [46]. Dedicated force fields were used for protein (ff99SBonlysc), lipids (lipid14), ions (ionsff99_tip3p) and water (TIP3P) [48]. MD simulations were performed at 300 K, with time step of 2 fs and in anisotropic pressure scaling conditions. Van der Waals and short-range electrostatic interactions were cut off at 10 Å, whilst long-range ones were computed with Particle Mesh Ewald (PME) method. Simulations were carried out for 100 ns for each system.

4.8.2. Molecular Docking

The crystal structures and the centroid of the most representative cluster obtained from MD simulations were used to dock ligands into S1R and AChE binding pockets. Ligand docking was carried out with Glide, a grid-based algorithm implemented in Maestro Schrödinger's suite [49]. The

grid was generated around the co-crystallized ligands with a radius of 15 Å. Default Van der Waals scaling was used, with scaling factor of 1.0 and partial change cut-off of 0.25. Partial charges were computed with the OPLS-2005 force field. E172 was selected as possible H-bond constraint for S1R ligand binding. Ligands of the training set were extracted from the ChEMBL database [50] and decoys from the DUDE database [51]. The S1R dataset included 102 agonists and 150 decoys. Whereas, for the AChE dataset we considered 100 inhibitors and 151 decoys. Ligands were processed with Maestro LigPrep, which generated three-dimensional structures and determined the protonation state. Rigid docking was performed for S1R by using a diverse set of 25 conformers for every molecule, which were generated by Maestro ConfGen with default settings. In contrast, flexible docking was applied to AChE ligands. The docking models were then validated with the new dataset of compounds that we present in this paper.

4.9. Antioxidant activity

FRS activity of the examined compounds was determined using the DPPH assay [42]. Briefly, compounds **8**, **10**, **13-14**, **18-20**, **23-28**, (R)-RC-33, Donepezil and Cur were dissolved in 1 mL of EtOH, to obtain a stock solution of 5.0 mM. The FRS potential was evaluated at a final concentration of 465 μM. The reaction mixture was prepared by adding 100 μL of each compound solution to 1.875 mL of DPPH solution, freshly prepared by dissolving DPPH in methanol/KH_2PO_4 and NaOH buffer (50/50 v/v) at a concentration of 6 x 10^{-5} M. After 20 min of incubation at room temperature, the absorbance was measured at 515 nm by the UV-Visible spectrophotometer.

FRS% was expressed as a percent compared with the control, consisting of 1.875 mL of DPPH solution and 100 μL of EtOH. The percent inhibition of the DPPH radical by the test solution was calculated using the following formula:

FRS%= [(Abs control – Abs sample) / Abs control] x100

The analyses were carried out in triplicate and results are expressed as mean ± SE.

4.10. MTS Assay

CellTiter 96® AQueous One Solution Cell Proliferation Assay (Promega, Milan, Italy) was used on cells seeded onto a 96-well plate at a density of 9×10^3 cells per well. The effect of compounds **8**, **10**, **13-14**, **18-20**, **23-28**, (R)-RC-33, donepezil and Cur was evaluated, at three different concentrations (10, 25 and 50 μM), after 24 h and 48 h of continued exposure. Three independent experiments were performed for each concentration. The optical density (OD) of treated and untreated cells was determined at a wavelength of 490 nm using a plate reader. For compounds **10**, **14** and **20**, a dose response curve was determined by using five different concentrations (1, 10, 25, 35, 50 and 100 μM). IC_{50} values were calculated by GrapH Pad Prism 5 Program.

4.11. Neuroprotection against H_2O_2 induced neurotoxicity

ROS assay was performed in living cells. Human neuroblastoma cell lines (SH-SY5Y) were seeded at 2×10^4 cells per well in 96-well plates for neuroprotection activity assay. Briefly, intracellular ROS production was measured from SH-SY5Y cells, using ab113851 kit (DCDFA ROS assay kit). Cells were pre-treated with compounds **10**, **14**, **20**, Cur, Donepezil and (R)-RC-33 for 3 h. The medium was replaced with 100 μL of DCDFA (25 μM) and incubated for 45 min. Afterwards the medium was eliminated and cells were washed with buffer solution. Lastly, cells were treated with 100 μL of each compound (10 μM) and H_2O_2 (180 μM) for 24 h. The total fluorescence was measured using a fluorescence microplate reader (Synergy HTX, Biotek), with excitation and emission wavelengths of 490 nm and 530 nm, respectively.

4.12. Neurotrophic activity

The neurotrophic activity was assessed by measuring the neurite elongation in DRG explants as experimental model. Briefly, compound 10 and 20 were dissolved in DMSO to obtain a stock solution of 10mM, then diluted in culture medium to obtain the different working concentrations. DRG from E15 Sprague-Dawley rats were aseptically removed and cultured onto a single layer of rat-tail collagen surfaces in 35mm dishes. DRG were incubated in AN_2 medium (MEM plus 10% Calf Bovine Serum, 50 µg/ml ascorbic acid, 1.4 mM L-glutamine, 0.6 % glucose) in the presence of 5ng/ml NGF and Fudr (10^{-5} M) to remove supporting cells in a 5% CO_2 humidified incubator at 37°C.

To study the neurotrophic effect of compound 10 and 20 on neurite elongation, DRG explants were treated for 2 hours with NGF and then exposed to different compound concentrations (10µM, 7,5 µM, 5 µM, 2,5 µM, 1µM, 750nM, 500nM, 250nM,) for 24 hours and 48 hours. DRG treated with AN_2 medium and 5ng/ml NGF alone represented controls. The neurotrophic effect was evaluated by measuring the length of the longest neurite in each DRG using the ImageJ program (NIH, Bethesda, MD, USA). A statistical analysis was carried out with the one-way Anova test and Tukey post-test with the statistical package GraphPad Prism (GraphPad Software, San Diego, CA, USA). P Value <0.05 was considered as statistically significant.

6. References

[1] Gao, H.M.; Hong, J.S. Why neurodegenerative diseases are progressive: uncontrolled inflammation drives disease progression. Trends Immunol. 29 (2008) 357–365.

[2] Golpich, M.; Amini, E.; Mohamed, Z.; Azman Ali, R.; Mohamed Ibrahim, N.; Ahmadiani, A. Mitochondrial Dysfunction and Biogenesis in Neurodegenerative diseases: Pathogenesis and Treatment. CNS Neurosci. Ther. 23 (2017) 5-22.

[3] Neurological disorders affect millions globally: WHO report. http://www.who.int/mediacentre/news/releases/2007/pr04/en/ (Accessed 07 April 2018).

[4] Kovacic, P.; Somanathan, R. Redox Processes in Neurodegenerative Disease Involving Reactive Oxygen Species. Curr. Neuropharmacol. 10 (2012) 289–302.

[5] Nowacek, A.; Kosloski, L.M.; Gendelman, H.E. Neurodegenerative disorders and nanoformulated drug development. Nanomedicine (Lond). 4 (2009) 541–555.

[6] Gitler, A.D.; Dhillon, P.; Shorter, J. Neurodegenerative disease: models, mechanisms, and a new hope. Dis. Model Mech. 10 (2017) 499–502.

[7] De Felice, A.; Ricceri, L.; Venerosi, A.; Chiarotti, F.; Calamandrei, G. Multifactorial Origin of Neurodevelopmental Disorders: Approaches to Understanding Complex Etiologies. Toxics. 3 (2015) 89–129.

[8] Cacabelos, R.; Fernandez-Novoa, L.; Lombardi, V.; Kubota, Y.; Takeda, M. Molecular genetics of Alzheimer's disease and aging. Methods Find Exp. Clin. Pharmacol. 27 (2005) Suppl A:1-573.

[9] Myhrer T. Neurotransmitter systems involved in learning and memory in the rat: a meta-analysis based on studies of four behavioral tasks. Brain Res. Brain Res. Rev. 41 (2003) 268-287.

[10] Perez-Lloret, S.; Barrantes, F.J. Deficits in cholinergic neurotransmission and their clinical correlates in Parkinson's disease. NPJ Parkinsons Dis. 2 (2016) 16001.

[11] Jucker, M.; Walker, L.C. Pathogenic Protein Seeding in Alzheimer’s Disease and Other Neurodegenerative Disorders. Ann, Neurol. 70 (2011) 532–540.

[12] Sweeney,P.; Park, H.; Baumann, M.; Dunlop, J.; Frydman, J.; Kopito, R.; McCampbell, A.; Leblanc, G.; Venkateswaran, A.; Nurmi, A.; Hodgson, R. Protein misfolding in neurodegenerative diseases: implications and strategies. Transl. Neurodegener. 6 (2017) 6.

[13] Chen, X.; Guo, C.; Kong, J. Oxidative stress in neurodegenerative diseases. Neural Regen. Res. 7 (2012) 376–385.

[14] Guo, C.; Sun, L.; Chen, X.; Zhang, D. Oxidative stress, mitochondrial damage and neurodegenerative diseases. Neural Regen. Res. 8 (2013) 2003–2014.

[14] Grant, P.; Song, J.Y.; Swedo, S.E. Review of the Use of the Glutamate Antagonist Riluzole in Psychiatric Disorders and a Description of Recent Use in Childhood Obsessive-Compulsive Disorder. J. Child Adolesc. Psychopharmacol. 20 (2010) 309–315.

[15] (a) Rossi, D.; Pedrali, A.; Gaggeri, R.; Marra, A.; Pignataro, L.; Laurini, E.; DalCol, V.; Fermeglia, M.; Pricl, S.; Schepmann, D.; Wünsch, B.; Peviani, M.; Curti, D.; Collina, S. Chemical, pharmacological, and in vitro metabolic stability studies on enantiomerically pure RC-33 compounds: promising neuroprotective agents acting as σ1 receptor agonists. Chem. Med. Chem. 8 (2013) 1514-1527. (b) Rossi, D.; Pedrali, A.; Marra, A.; Pignataro, L.; Schepmann, D.; Wünsch, B.; Ye, L.; Leuner, K.; Peviani, M.; Curti, D.; Azzolina, O.; Collina, S. Studies on the enantiomers of RC-33 as neuroprotective agents: isolation, configurational assignment, and preliminary biological profile. Chirality 25 (2013) 814-822. (c) Marra, A.; Rossi, D.; Pignataro, L.; Bigogno, C.; Canta, A.; Oggioni, N.; Malacrida, A.; Corbo, M.; Cavaletti, G.; Peviani, M.; Curti, D.; Dondio, G.; Collina, S. Toward the identification of neuroprotective agents: g-scale synthesis, pharmacokinetic evaluation and CNS distribution of (R)-RC-33, a promising Sigma1 receptor agonist. Future Med. Chem. 8 (2016) 287-295.

[16] Collina, S.; Rui, M.; Stotani, S.; Bignardi, E.; Rossi, D.; Curti, D.; Giordanetto, F.; Malacrida, A.; Scuteri, A.; Cavaletti, G. Are sigma receptor modulators a weapon against multiple sclerosis disease? Future Med. Chem. 9 (2017) 2029-2051.

[17] Geldenhuys, W.J.; Van der Schyf, C.J. Rationally designed multi-targeted agents against neurodegenerative diseases. Curr. Med. Chem. 20 (2013) 1662-1672.

[18] Nguyen, L.; Lucke-Wold, B.P.; Mookerjee, S.; Kaushal, N.; Matsumoto, R.R. Sigma-1 Receptors and Neurodegenerative Diseases: Towards a Hypothesis of Sigma-1 Receptors as Amplifiers of Neurodegeneration and Neuroprotection. Adv. Exp. Med. Biol. 964 (2017) 133-152.

[19] Collina, S.; Gaggeri, R.; Marra, A.; Bassi, A.; Negrinotti, S.; Negri, F.; Rossi, D. Sigma receptor modulators: a patent review. Exp. Opin. Ther. Patent 23 (2013) 597-613.

[20] Ruscher, K.; Wieloch, T. The involvement of the sigma-1 receptor in neurodegeneration and neurorestoration. J. Pharmacol. Sci. 127 (2015) 30-35.

[21] Nguyen, L.; Lucke-Wold, B.P.; Mookerjee, S.A.; Cavendish, J.Z.; Robson, M.J.; Scandinaro, A.L.; Matsumoto, R.R. Role of sigma-1 receptors in neurodegenerative diseases. J. Pharmacol. Sci. 127 (2015) 17-29.

[22] Penke, B.; Fulop, L.; Szucs, M.; Frecska, E. The Role of Sigma-1 Receptor, an Intracellular Chaperone in Neurodegenerative Diseases. Curr. Neuropharmacol. 16 (2018) 97-116.

[23] Weng, T.Y.; Tsai, S.Y.A.; Su, T.P. Roles of sigma-1 receptors on mitochondrial functions relevant to neurodegenerative diseases. J. Biomed. Sci. 24 (2017) 74.

[24] Tsai, S.Y.; Hayashi, T.; Mori, T.; Su, T.P. Sigma-1 Receptor Chaperones and Diseases. Cent. Nerv. Syst. Agents Med. Chem. 9 (2009) 184–189.

[25] Čolović, M.B.; Krstić, D.Z.; Lazarević-Pašti, T.D.; Bondžić, A.M.; Vasić, V.M. Acetylcholinesterase Inhibitors: Pharmacology and Toxicology. Curr. Neuropharmacol. 11 (2013) 315–335.

[26] Holzgrabe, U.; Kapková, P.; Alptüzün, V.; Scheiber, J.; Kugelmann, E. Targeting acetylcholinesterase to treat neurodegeneration. Expert Opin. Ther. Targets. 11 (2007) 161-179.

[27] Barzegar, A.; Moosavi-Movahedi, A.A. Intracellular ROS protection efficiency and free radical-scavenging activity of curcumin. PLoS One. 6 (2011) e26012.

[28] Herbal Medicine: Biomolecular and Clinical Aspects. 2nd edition. Chapter 13 Turmeric, the Golden Spice. Benzie IFF, Wachtel-Galor S, editors. Boca Raton (FL): CRC Press/Taylor & Francis (2011).

[29] Anand, P.; Kunnumakkara, A.B.; Newman, R.A.; Aggarwal, B.B. Bioavailability of Curcumin: Problems and Promises. Mol. Pharmaceutics 4 (2007) 807-818.

[30] Cole, G.M.; Teter, B.; Frautschy, S.A. Neuroprotective effects of Curcumin. *A*dv. Exp. Med. Biol. 595 (2007) 197–212.

[31] Monroy, A.; Lithgow, G.J.; Alavez, S. Curcumin and neurodegenerative diseases. Biofactors. 39 (2013) 122-32.

[32] Amalraj, A.; Pius, A.; Gopi, S.; Gopi, S. Biological activities of curcuminoids, other biomolecules from turmeric and their derivatives – A review. J. Tradit. Complement. Med. 7 (2017) 205–233.

[33] Muehlbacher, M.; Spitzer, G.M.; Liedl, K.R.; Kornhuber, J. Qualitative prediction of blood-brain barrier permeability on a large and refined dataset. J. Comput. Aided Mol. Des. 25 (2011) 1095-106.

[34] Wager, T.T.; Hou, X.; Verhoest, P.R.; Villalobos, A. Central Nervous System Multiparameter Optimization Desirability: Application in Drug Discovery. ACS Chem. Neurosci. 7 (2016) 767-775.

[35] Temme, L.; Frehland, B.; Schepmann, D.; Robaa, D.; Sippl, W.; Wünsch, B. Hydroxymethyl bioisosteres of phenolic GluN2B-selective NMDA receptor antagonists: Design, synthesis and pharmacological evaluation. Eur. J. Med. Chem. 144 (2018) 672-681.

[36] Ellman, G.L.; Courtney, K.D.; Andres, V.; Feather-Stone, R.M. A new and rapid colorimetric determination of acetylcholinesterase activity. Biochem. Pharmacol. 7 (1961) 88-95.

[37] Mishra, C.B.; Manral, A.; Kumari, S.; Saini, V.; Tiwari, M. Design, synthesis and evaluation of novel indandione derivatives as multifunctional agents with cholinesterase inhibition, anti-β-amyloid

aggregation, antioxidant and neuroprotection properties against Alzheimer's disease. Bioorg. Med. Chem. 24 (2016) 3829-3841.

[38] Meunier, J.; Ieni, J.; Maurice, T. The anti-amnesic and neuroprotective effects of donepezil against amyloid beta25–35 peptide-induced toxicity in mice involve an interaction with the sigma1 receptor. Br. J. Pharmacol. 149 (2006) 998–1012.

[39] Phaniendra, A.; Jestadi, D.B.; Periyasamy, L. Free Radicals: Properties, Sources, Targets, and Their Implication in Various Diseases. Indian J. Clin. Biochem. 30 (2015) 11–26.

[40] Fetisova, E.; Chernyak, B.; Korshunova, G.; Muntyan, M.; Skulachev, V. Mitochondria-targeted Antioxidants as a Prospective Therapeutic Strategy for Multiple Sclerosis. Curr. Med. Chem. 24 (2017) 2086-2114.

[41] Schmidt, H.R., Zheng, S.D., Gurpinar, E., Koehl, A., Manglik, A., and Kruse, A.C. Crystal structure of the human sigma 1 receptor. Nature 532 (2016) 527-530.

[42] Berman, H.M., Westbrook, J., Feng, Z., Gilliland, G., Bhat, T.N., Weissig, H., Shindyalov, I.N., and Bourne, P.E. The Protein Data Bank. Nucleic Acids Research 28 (2000) 235-242.

[43] Cheung, J., Rudolph, M.J., Burshteyn, F., Cassidy, M.S., Gary, E.N., Love, J., Franklin, M.C., and Height, J.J. Structures of Human Acetylcholinesterase in Complex with Pharmacologically Important Ligands. J. Med. Chem. 55 (2012) 10282-10286.

[44] Molecular Operating Environment (Moe) (2016). 2015.1001 ed. (Montreal, QC, Canada: Chemical Computing Group Inc.).

[45] Jo, S., Kim, T., and Im, W. Automated builder and database of protein/membrane complexes for molecular dynamics simulations. *PLoS One* 2 (2007) e880.

[46] D.A. Case, V.B., J.T. Berryman, R.M. Betz, Q. Cai, D.S. Cerutti, T.E. Cheatham, Iii, T.A. Darden, R.E. Duke, H. Gohlke, A.W. Goetz, S. Gusarov, N. Homeyer, P. Janowski, J. Kaus, I. Kolossváry, A. Kovalenko,, T.S. Lee, S.L., T. Luchko, R. Luo, B. Madej, K.M. Merz, F. Paesani,

D.R. Roe, A. Roitberg, C. Sagui, R. Salomon-Ferrer, G. Seabra, C.L. Simmerling, W. Smith, J. Swails, R.C. Walker, J. Wang, R.M. Wolf, X., and Kollman, W.a.P.A. (2014). AMBER 14.

[47] Wang, J.M., Wang, W., Kollman, P.A., and Case, D.A. Automatic atom type and bond type perception in molecular mechanical calculations. Journal of Molecular Graphics & Modelling 25 (2006) 247-260.

[48] Dickson, C.J., Madej, B.D., Skjevik, A.A., Betz, R.M., Teigen, K., Gould, I.R., and Walker, R.C. Lipid14: The Amber Lipid Force Field. J. Chem. Theory Comput. 10 (2014) 865-879.

[49] Friesner, R.A., Banks, J.L., Murphy, R.B., Halgren, T.A., Klicic, J.J., Mainz, D.T., Repasky, M.P., Knoll, E.H., Shelley, M., Perry, J.K., Shaw, D.E., Francis, P., and Shenkin, P.S. Glide: a new approach for rapid, accurate docking and scoring. 1. Method and assessment of docking accuracy. J. Med. Chem. 47 (2004) 1739-1749.

[50] Bellis, L.J., Gaulton, A., Hersey, A., Bento, A.P., Chambers, J., Davies, M., Kruger, F., Light, Y., Dedman, N., Mcglinchey, S., Nowotka, M., Papadatos, G., Santos, R., and Overington, J.P. (2014). ChEMBL - linking chemistry and biology to enable mapping onto molecular pathways. Abstracts of Papers of the American Chemical Society 248.

[51] Mysinger, M.M., Carchia, M., Irwin, J.J., and Shoichet, B.K. Directory of Useful Decoys, Enhanced (DUD-E): Better Ligands and Decoys for Better Benchmarking. *J. Med. Chem.* 55 (2012) 6582-6594.